Space Sci Rev (2007) 132: 229–260
DOI 10.1007/s11214-007-9228-9

Interior Evolution of Mercury

Doris Breuer · Steven A. Hauck II · Monika Buske · Martin Pauer · Tilman Spohn

Received: 9 February 2007 / Accepted: 30 May 2007 / Published online: 26 October 2007

Abstract The interior evolution of Mercury—the innermost planet in the solar system, with its exceptional high density—is poorly known. Our current knowledge of Mercury is based on observations from Mariner 10's three flybys. That knowledge includes the important discoveries of a weak, active magnetic field and a system of lobate scarps that suggests limited radial contraction of the planet during the last 4 billion years. We review existing models of Mercury's interior evolution and further present new 2D and 3D convection models that consider both a strongly temperature-dependent viscosity and core cooling. These studies provide a framework for understanding the basic characteristics of the planet's internal evolution as well as the role of the amount and distribution of radiogenic heat production, mantle viscosity, and sulfur content of the core have had on the history of Mercury's interior.

The existence of a dynamo-generated magnetic field suggests a growing inner core, as model calculations show that a thermally driven dynamo for Mercury is unlikely. Thermal evolution models suggest a range of possible upper limits for the sulfur content in the core. For large sulfur contents the model cores would be entirely fluid. The observation of limited planetary contraction (∼1–2 km)—if confirmed by future missions—may provide a lower limit for the core sulfur content. For smaller sulfur contents, the planetary contraction obtained after the end of the heavy bombardment due to inner core growth is larger than the observed value. Due to the present poor knowledge of various parameters, for example, the mantle rheology, the thermal conductivity of mantle and crust, and the amount and distribution of radiogenic heat production, it is not possible to constrain the core sulfur content nor

D. Breuer (✉) · M. Pauer · T. Spohn
DLR, Institut für Planetenforschung, Berlin, Germany
e-mail: doris.breuer@dlr.de

M. Pauer
Department of Geophysics, Charles University of Prague, Prague, Czech Pepublic

S.A. Hauck II
Department of Geological Sciences, Case Western Reserve University, Cleveland, OH 44106, USA

M. Buske
Max-Planck Institut für Sonnensystemforschung, Lindau, Germany

the present state of the mantle. Therefore, it is difficult to robustly predict whether or not the mantle is conductive or in the convective regime. For instance, in the case of very inefficient planetary cooling—for example, as a consequence of a strong thermal insulation by a low conductivity crust and a stiff Newtonian mantle rheology—the predicted sulfur content can be as low as 1 wt% to match current estimates of planetary contraction, making deep mantle convection likely. Efficient cooling—for example, caused by the growth of a crust strongly in enriched in radiogenic elements—requires more than 6.5 wt% S. These latter models also predict a transition from a convective to a conductive mantle during the planet's history. Data from future missions to Mercury will aid considerably our understanding of the evolution of its interior.

Keywords Mercury · Mantle convection · Thermal evolution · Volcanic activity

1 Introduction

Mercury, the innermost planet, is the least-explored planet in the solar system, yet one of the most interesting and puzzling ones, even in comparison with Pluto (regardless of Pluto's reclassification as a dwarf planet by the International Astronomical Union in 2006). Mercury was visited by the Mariner 10 spacecraft in 1974–1975 during three flybys. Data from this mission, though limited and variable in resolution, together with some earth-based observations (e.g., Sprague et al. 1994, 1997; Anderson et al. 1996; Harmon 1997) helped to improve our understanding of Mercury. Here we review the present state of knowledge of the interior evolution of the planet. We begin by summarizing relevant spacecraft and Earth-based observations of Mercury and their implications for the evolution of the interior.

Surface: The known hemisphere of Mercury is similar to the Moon; the morphologies of both surfaces are dominated by craters and are roughly 4 Ga old. Based on infrared spectral data, Sprague et al. (1994, 1997) proposed that Mercury may have an anorthosite-rich crust that formed as a flotation crust on a magma ocean just like the highlands crust on the Moon. The low iron content of the surface suggests that Mercury may be more differentiated than the other terrestrial planets (Vilas 1988). The intercrater plains, which are the most widespread surface type, are thought to have been formed by a global resurfacing event before the end of the late heavy bombardment, 4 to 4.2 Ga. However, no unambiguous evidence of volcanic activity, such as domes or rilles, has been observed, possibly due to the lack of high-resolution data. The wide distribution of basin ejecta has been proposed as an alternative mechanism for resurfacing, but no source is visible on the observed hemisphere. Lobate scarps resulting from thrust faults, and a lack of significant extensional faulting, indicates a contraction of the planetary radius by 1 to 2 km (e.g., Strom et al. 1975; Watters et al. 1998) since the end of the heavy bombardment, which was most likely induced by the cooling of Mercury's mantle and the partial freezing of its core.

Interior structure: The Mariner 10 flybys revealed that Mercury has an average density of 5,430 $\mathrm{kg\,m^{-3}}$ (Anderson et al. 1987), which suggests a relative core radius, R_c/R_P, of about 0.8 and thus a thin mantle shell of only about 600 km thickness (e.g., Spohn et al. 2001; Harder and Schubert 2001; Van Hoolst et al. 2007, this issue). The core may actually comprise the entire planet if a pure FeS core composition is assumed (Harder and Schubert 2001). By comparison, the Moon has a $R_c/R_P < 0.25$–0.3 and Mars and Earth have core radii of about half the surface radius. A value of $R_c/R_P \sim 0.5$ is also consistent with the bulk density of Venus despite not being uniquely constrained, as well as data for Io and Ganymede, after removal of the ice layer of the latter. The crustal thickness of Mercury crust

is loosely constrained by a combination of results from Earth-based radar topography data and Mariner 10 gravity data that suggest a thickness of 100–300 km (Anderson et al. 1996). Studies employing stereo topographical information about the Mercurian surface (Nimmo and Watters 2004; Watters et al. 2004) suggest that the extensional faulting of observed lobate scarps is consistent with a mean crustal thickness of 90–140 km.

Magnetic field: Mercury features an internal magnetic field, which is rivaled in strength only by the Earth and Ganymede among solid bodies in the solar system. The internal field was measured during only two flybys of the Mariner 10 mission in 1974 and 1975 on its way to Mars and is therefore not very well known. The dipole moment calculated from the data of 4.9×10^{12} T m^3 is about three orders of magnitude smaller than that of the Earth field and the field strength at the equator is estimated to be about 350 nT or 1/100 of that of the Earth (Ness et al. 1974). The discovery of the internal field strongly suggests the presence of a fluid outer core (e.g., Stevenson et al. 1983) although a crustal source of the measured field cannot be excluded at present (Aharonson et al. 2004).

To understand the interrelation between various observations, in particular the existence of a weak magnetic field, the small amount of planetary contraction, and the thin mantle, a comprehensive study of the interior dynamics and of related processes is required. Fundamentally, the internal dynamics of terrestrial bodies are driven by the transport of heat from the interior to the surface. Heat generation and transport are the processes which connect the structure and chemistry of a planetary body with its dynamical behaviour, such as mantle convection, volcanism, tectonism, and magnetic field generation. The physical and chemical properties of planetary materials influence the mechanics of the planetary heat engine driving dynamics, while the dynamics in turn alter the physical and chemical properties of the planet's interior.

The interactions between various processes have been studied with thermal and thermo-chemical evolution models (e.g., Stevenson et al. 1983; Schubert et al. 1988; Hauck et al. 2004). In this paper, we review these models and also present some first results of 2D and 3D thermal convection models. The paper begins with a detailed description of the important observational constraints, such as estimates of the global contraction and heat flow, the crustal thickness and composition, and the magnetic field. In the next section we describe the main heat transport mechanisms relevant for Mercury, conductive and convective heat transport. For the latter heat transport mechanism, we introduce the main analytical tools, finite amplitude and parameterized convection models, as well as the relevant parameters and initial thermal conditions to calculate mantle dynamics and the thermal evolution. Then we discuss results for dynamics of Mercury's mantle and the thermo-chemical evolution of the mantle and core, including magnetic field generation. The chapter ends with a summary and a discussion of what we will learn from the upcoming missions with respect to the interior evolution of Mercury.

2 Observational Constraints on Thermal History Models

2.1 Planetwide Contraction and Heat Flow

One of the most significant outcomes of the Mariner 10 mission was the idea that Mercury's surface may hold a tectonic record directly related to the planet's cooling history (e.g., Strom et al. 1975; Solomon 1976; Cordell and Strom 1977; Solomon 1977). This concept is the result of the discovery of a prominent and curious set of tectonic features known as lobate scarps, which are asymmetric, arcuate, scarps that are 10–100's of kilometers long with

relief of up to a kilometer or more (e.g., Strom et al. 1975; Watters et al. 1998) and are interpreted to be the surface expression of thrust faults. Due to the apparently random locations and orientations of lobate scarps (e.g., Strom et al. 1975; Cordell and Strom 1977) they have been interpreted to have been formed as a result of global contraction of the planet (Strom et al. 1975; Watters et al. 1998). Though recent work as reopened the idea that the scarps have some distinct orientation (Watters et al. 2004) the global contraction hypothesis remains viable because planetary lithospheres are rarely homogeneous and global contraction may be one of several sources of stress superimposed on Mercury's lithosphere. Lobate scarp formation is inferred to have begun after heavy bombardment and continued through smooth plains formation based on the observation that the scarps are not embayed by intercrater plains material (e.g., Cordell 1977; Strom 1997) and that they deform several large craters as well as smooth plains material, which makes up the youngest geologic unit on Mercury (Strom et al. 1975; Cordell 1977; Cordell and Strom 1977; Spudis and Guest 1988). Structural analysis of lobate scarps has deduced that they record ∼0.05–0.10% strain that in turn reflects approximately 1–2 km reduction in radius since the end of the heavy bombardment, with recent estimates favouring the low end of this range (Strom et al. 1975; Watters et al. 1998). Global contraction is likely the result of net cooling of the planet's interior, which leads to contraction through a decrease in internal temperatures and phases changes such as that associated with the solidification of an inner core (e.g., Solomon 1976, 1977; Schubert et al. 1988; Hauck et al. 2004). Cooling and complete solidification of a pure metallic iron core from an initially molten state would result in a ∼17 km decrease in radius (Solomon 1976), in contrast with observations. Mercury's modest amount of inferred contraction may either require a mechanism to strongly limit planetary cooling or, conversely, additional manifestations of global contraction not included in current estimates (e.g., Hauck et al. 2004).

The largest lobate scarp on the hemisphere imaged by Mariner 10, Discovery Rupes, is >500 km in length has also been used to estimate the paleo heat flow on Mercury (Watters et al. 2002). This thrust fault is assumed to have cut the entire elastic and seismogenic lithosphere when it formed (∼4.0 Gyr ago). On Earth, the maximum depth of faulting is thermally controlled. Assuming the limiting isotherm for Mercury's crust is ∼600 to 900 K and it occurred at a depth of about 40 km, the corresponding heat flux at the time of faulting was ∼10 to 43 $\mathrm{mW\,m^2}$. This is less than the heat flow in the old terrestrial oceanic lithosphere but greater than the present heat flux on the Moon. The results by Watters et al. (2002) strongly depend on the accuracy of the measured topography, which was derived from digital stereoanalysis of Mariner 10 imagery (Watters et al. 1998; Cook and Robinson 2000), using updated camera orientations (Robinson et al. 1999). The errors in the data are large and better estimates on the paleo heat flow, including those from different locations, can be obtained when gravity and topographic data are available from MESSENGER (Solomon et al. 2001) and BepiColombo (Grard and Balogh 2001).

2.2 Crust Thickness and Composition

Mercury's crust holds potentially important clues to the planet's internal evolution. In particular, the history and magnitude of crustal production, as well as its composition, may provide information on thermal history of the interior. Ground radar measurements performed between 1967 and 1990 provided an estimate of the global shape of Mercury—among other parameters the equatorial flattening of Mercury was determined to be $(540 \pm 54) \times 10^{-6}$ (Anderson et al. 1996). This together with Mariner 10 flyby gravity measurement of $C_{22} = (1.55 \pm 0.77) \times 10^{-5}$ (Anderson et al. 1987) was used to constrain the mean crustal

thickness to be 200 ±100 km under the assumption of full isostatic compensation (Anderson et al. 1996). However, the approach used to obtain the crustal thickness seems to be uncertain since it does not give realistic values of the mean crustal thickness for Mars (Anderson et al. 1996) or (with updated values of equatorial flattening from the Clementine laser altimetry experiment (Smith et al. 1997)) for the Moon.

Another approach to constraining the mean crustal thickness is based on analysis of tectonic structures and their topographic relief. The assumed depth of faulting of the lobate scarps (elongated thrust faults presumably originated from the planetary contraction) of 30–40 km (Watters et al. 2002) suggests that irrespective of the crustal heat generation the mean crustal thickness at the time of the formation of the lobate scarps was ≤140 km and the effective elastic thickness 25–30 km (Nimmo and Watters 2004). Similar limits on the crustal thickness have been estimated by the study of topographic profiles of extensional troughs in Caloris basin. These troughs have a shape consistent with lateral flow of a dry plagioclase lower crust with a total crustal thickness of 90–140 km producing 70–90% topographical relaxation within likely limits of radiogenic heat flux (Watters et al. 2005).

Each estimate represents a broad range and new, more accurate gravity, topography, and stereo imagery data from MESSENGER and BepiColombo may substantively revise these results. Regardless, the total volume of crust represents some combination of primary crust, the result of crystal–liquid separation in a primordial silicate magma ocean, and secondary crust, derived from partial melting of the mantle. The persistence of a primary crust depends principally on any primary crust not being removed either by external sources such as a giant impact (e.g., Cameron et al. 1988; Wetherill 1988) or vaporization of the surface (Fegley and Cameron 1987) or internally by crustal recycling. Existence of a primordial crust is supported by reflectance spectra of the surface of Mercury. Those spectra are similar to that of the lunar highlands (Vilas 1988; Sprague et al. 1997), which are predominately plagioclase and were most likely formed by freezing of a magma ocean. Furthermore, the radar characteristics of Mercury's surface are also reminiscent of the lunar highlands (Harmon 1997). As the time-integrated result of mantle partial melting, the secondary crust provides information on the thermal history and composition of the mantle and hence can be compared in a relatively straightforward manner with models of the planet's thermal history (e.g., Hauck et al. 2004). Though the relative fraction of primary to secondary crust on Mercury is unknown, the total crustal thickness can provide an absolute upper bound on the amount of secondary crust produced by the mantle. At present, there are too few data on the composition of Mercury's crust—beyond inferences of a low FeO content (e.g., Jeanloz et al. 1995; Robinson and Taylor 2001) and its similarity to anorthositic lunar crust—to provide any significant constraints on the history of Mercury's interior. However, future determinations of surface mineralogy and the concentrations of heat-producing elements could provide important information for modelling efforts.

2.3 Magnetic Field

Magnetic field generation in the iron core of a planet is strongly coupled to the thermal evolution of the planet. Thus, knowledge about the magnetic field evolution can be used to constrain the planet's thermal evolution. During its first and third close encounters in with Mercury 1974 and 1975, Mariner 10 passed briefly through, and measured a small, but Earth-like, magnetosphere. The analyses of these observations revealed the presence of an internal field, with a dipole moment that is a factor of about 10^4 smaller than that of the Earth (Ness et al. 1974; Russel et al. 1988; see also the review in Connerney and Ness 1988). Prior to the detection of the magnetic field, it had been assumed that Mercury's core froze early in the planet's history; however, this assumption is not consistent

with the idea that the field is the result of dynamo action in the core. The discovery of the internal field strongly suggests the presence of a fluid outer core, although a crustal source of the measured field cannot be excluded at present (Aharonson et al. 2004), nor can the more exotic proposal of a thermoelectric dynamo (Stevenson 1987; Giampieri and Balogh 2002). To prevent the core from freezing, the addition of radioactive heat sources into the core (e.g., Toksöz et al. 1978) or late core formation (e.g., Sharpe and Strangway 1976; Solomon 1977) have been suggested. A late core formation would support a cool initial state for Mercury but is at variance with accretion models (e.g., Schubert et al. 1988). However, the most likely reason for Mercury not having a totally frozen core is the incorporation of a light alloying element into its core that reduces the core melting temperature. Here, sulfur is the most likely candidate (Ringwood 1977; McCammon et al. 1983). The amount of sulfur depends on the accretion and formation scenario of Mercury. In the most conservative equilibrium condensation models there is no sulfur at all in Mercury's core (Lewis 1972; Grossman 1972), an assumption often used in earlier thermal evolution models (e.g. Siegfried and Solomon 1974; Sharpe and Strangway 1976; Solomon 1976, 1977). However, a low concentration of sulfur has been suggested due to radial mixing of planetesimals and/or nonequilibrium condensation models (Basaltic Volcanism Study Project 1981; Wetherill 1985). That Mercury's inner structure is consistent with its high density can actually be explained by a wide range of the sulfur concentration in the core, ranging from a pure iron core to a core with a pure iron sulfide composition (Harder and Schubert 2001).

A necessary condition for generating a self-sustained, hydromagnetic dynamo is convection in a fluid or partly fluid core. Core convection can basically occur in two ways.

(1) **Thermal convection** in the core, like thermal convection in the mantle, is driven by a sufficiently large super-adiabatic temperature difference between the core and the mantle. It occurs if the core heat flow exceeds that conducted along the core adiabat.
(2) **Compositional convection** can occur due to the release of positively buoyant material during the process of solid inner core freezing from a fluid core with non-eutectic composition (Braginsky 1964). Chemical convection and the associated generation of a magnetic field in the core occur if the temperature in the fluid (outer) core ranges between the solidus and the liquidus of the core material. Inner core growth permits outer core convection even when the heat flow through the core–mantle boundary is less than the heat carried by conduction along the adiabat. Furthermore, compositional convection is energetically more efficient at driving a dynamo because of the vagaries of a heat engine.

In either case, the core must be cooling and the cooling is controlled by the heat transport through the outer layers of the planet—mantle and crust. Thus, understanding the magnetic field history of Mercury also requires an understanding of the thermal evolution of the planet.

Current thermal evolution models for Mercury try to explain the present-day magnetic field in a fluid core—assuming that this field has a dynamo origin. Future missions will show whether this assumption is valid or whether the present magnetic field is due to remnant magnetization of the crust. Measurements of possible remnant magnetization of the crust are in any case of important for understanding the evolution of Mercury. It is assumed that the remnant magnetization can be established at the time of crust formation while an internal dynamo was active. An age determination of the magnetized and non-magnetized crust would thus allow us to reconstruct the magnetic field history as has been done for Mars (Acuña et al. 1999) and the Moon (Runcorn 1975). However, should Mercury have a present-day dynamo-generated field like the Earth, the separation of a possible additional remnant field might be difficult to establish from orbit, as would the reconstruction of the

magnetic field history. Such a reconstruction is more likely if Mercury's present field is caused by crust magnetization.

3 Modes of Heat Transfer

3.1 Conductive and Convective Heat Transport

In a terrestrial planet like Mercury there are basically two main mechanisms for the transfer of heat—conduction and convection. The conductive heat transfer is a diffusive process wherein molecules transmit their kinetic energy to other molecules by colliding with them. In a medium with a spatial variation of temperature, heat is conducted from the warmer region to the colder. The basic relation for linear conductive heat transport states that the heat flux is directly proportional to the temperature gradient and the thermal conductivity. The latter parameter is a bulk property of the material that indicates its ability to conduct heat. It depends on temperature, pressure, composition and structure of the material. In a convecting, one-plate planet, the upper mantle boundary layer, also known as the stagnant lid, transports heat by conduction. Beneath the stagnant lid heat is transported by convection.

Convective heat transport is associated with the motion of the material and is more efficient in transporting heat than conduction. In a convecting medium, hot fluid flows into a cold region and heats it. Similarly, a cold fluid flows into a hot region and cools it. The motion is caused by the temperature-induced density variations. As a hot fluid is less dense than a cold fluid of the same material, the flow pattern in a terrestrial planet shows, in general, hot uprising material and sinking cold material. Convection starts when the buoyancy forces due the thermal density variations are stronger than the resisting forces like the viscous drag and the thermal conductivity of the material. The ability and strength of the convection is usually described by the Rayleigh number, which is proportional to the cube of the layer thickness and inverse proportional to the mantle viscosity. Convection sets in when the Rayleigh number of a terrestrial mantle is larger than the critical Rayleigh number. The higher the Rayleigh number the stronger the convection and the more efficient the heat transport. In contrast, for a terrestrial mantle with a Rayleigh number lower than a critical Rayleigh number, heat is transported by conduction alone. Among others, the critical Rayleigh number depends on the aspect ratio of the mantle shell (core radius / planetary radius). The thinner a shell becomes, the smaller the critical Rayleigh number (Zebib et al. 1983). Thus, Mercury's mantle with an aspect ratio of about 0.8 has the lowest critical Rayleigh number of all the terrestrial planets; nonetheless, Mercury's small size leads to a low intrinsic Rayleigh number for the mantle. Whether and how long convection took place in Mercury will be discussed in the following. For the modelling of the heat transfer in a terrestrial planet in general two different approaches are used, parameterized convection and finite amplitude models.

3.2 Parameterized Models

Thermal evolution calculations with 2D or 3D mantle convection codes are still very time-consuming on present-day computers. Because of the inherent complexity in these models it is often desirable to take an empirical approach and parameterize the convective heat transfer rate as a function of known quantities. Such parameterizations can be derived using simple theories, which result in scaling laws that describe the heat transport in the interior. As an output, global parameters such as the mean mantle and core temperature, mean heat flow of

the mantle and core, and average mantle flow velocity can be obtained as a function of time (e.g., Stevenson et al. 1983; Schubert et al. 2001).

Our improved understanding of the heat transport mechanisms on terrestrial planets over the last two decades has led to repeated changes in the preferred scaling law used to model the thermal evolution of one-plate planets. Initially, the scaling law for a fluid with constant viscosity was used for one-plate planets (e.g., Stevenson et al. 1983). Since that time, it has been recognized that this scaling law models the heat transport in a planet where convection comprises the whole mantle, including the outer layers. In fact, such a model reasonably describes the heat transport in a planet with plate tectonics better than that in a one-plate planet (e.g., Schubert et al. 2001). The plate tectonic regime is expected to cool the planet very efficiently because the comparatively cold outer layers become recycled into the interior of the mantle by convection.

Subsequent attempts to model the heat transport in one-plate planets included the effects of a growing lithosphere in the models with parameterizations based on constant viscosity scaling laws (e.g., Schubert et al. 1990). The base of the non-convecting lithosphere is represented by a characteristic isotherm for the transition from viscous deformation to a rigid response to loads applied over geologic time scales (e.g., Schubert et al. 1992). Such a model represents the heat transport in a planet with a single plate on top of a convecting mantle. However, this model assumes that the lid coincides with the rheological lithosphere. The part of the upper mantle that is weaker than the rheological lithosphere is assumed to be constantly recycled within the mantle. In comparison to the recently derived stagnant lid parameterization, these models, therefore, represent a mechanism of lithospheric delamination. The efficiency of the heat transport by lithospheric delamination is in between that of plate tectonics and that of stagnant lid convection.

Recently, new scaling laws have been derived from convection models in layers of fluids with strongly temperature-dependent viscosities (e.g., Richter et al. 1983; Davaille and Jaupart 1993; Solomatov 1995; Moresi and Solomatov 1995; Grasset and Parmentier 1998; Reese et al. 1999; Solomatov and Moresi 2000). These scaling laws have been suggested to represent the heat transport in a planet with a single plate on top of a convecting mantle as it is assumed for Mercury. To model the thermal evolution of a one-plate planet with a stagnant lid parameterization, one solves the energy equation of the mantle and the core and uses the scaling law which relates the heat loss to the strength of the convection in the mantle. Detailed descriptions of the equations and the methods can be found in the literature, including the growth of a crust associated with a redistribution of the radioactive elements and the magnetic field evolution (Hauck and Phillips 2002; Hauck et al. 2004; Breuer and Spohn 2003, 2006).

3.3 Finite Amplitude Models

Finite amplitude models in 2D or 3D geometry provide detailed information on mantle dynamics and the associated heat transport via calculation of local parameters such as the temperature and velocity fields. In convection models mantle material is considered a highly viscous and incompressible fluid, which can be described by the equations of fluid dynamics. In the framework of the Boussinesq approximation, which is commonly used in thermal convection models, the mantle density is constant except for the buoyancy term (see Schubert et al. 2001). The conservation of mass, momentum and energy are given in the following non-dimensional equations:

$$\nabla \cdot \vec{u} = 0, \tag{1}$$

$$\nabla p = \nabla \cdot \left(\eta' \left(\nabla \vec{u} + \{\nabla \vec{u}\}^{\mathrm{T}}\right)\right) + Ra\, T \vec{e}_r, \tag{2}$$

$$\frac{\partial T}{\partial t} + \vec{u} \nabla T = \nabla^2 T + H, \tag{3}$$

where ∇ denotes the nabla operator, η' the viscosity, $\vec{u}$ the velocity vector, p the dynamic pressure, $\{\}^{\mathrm{T}}$ the tensor transpose, T the temperature and $\vec{e}_r$ the unit vector in radial direction. The Rayleigh number comparing the convection supporting and the impeding effects is defined as follows: $Ra = \alpha \rho_m^2 C_m g \Delta T d^3 / \eta_{\mathrm{ref}} \lambda$ with the thermal expansivity α, the thermal conductivity k, the density ρ_m, the heat capacity C_m of the mantle, the mantle or shell thickness d, the initial temperature contrast between the surface and the core mantle boundary ΔT, and g the acceleration of gravity. The dimensionless internal heating rate is denoted as $H = Q d^2 / \lambda \Delta T$ where Q is the volumetric heating rate (heat produced by the decay of radioactive elements), which decreases exponentially with time ($Q = Q_0 \exp(-\sigma t)$) with the decay rate σ and the initial value Q_0.

Although models of finite amplitude convection have improved in recent years, particularly with the consideration of complex rheologies and parallelization of the codes for efficiency in calculation times, to our knowledge only one 2D convection model with strongly temperature-dependent viscosity for Mercury has been published so far (Conzelmann 1999). We present 2D and preliminary 3D convection models in a spherical shell with temperature-dependent viscosity that also consider the cooling of the core and potential inner core growth. A detailed description of the model is given in the Appendix and the discussion of our results and how they compare with earlier studies is given in Sect. 5.

4 Early Conditions and Relevant Parameters for Thermo-Chemical Evolution

A challenge for modelling and understanding Mercury's internal evolution is a lack of knowledge of Mercury's early thermal conditions and of its chemical composition. The latter influences relevant parameters of the thermal evolution such as the amount of radioactive elements, the mantle rheology, and the thermal properties of the mantle and crust. Some, if not all, of these parameters, however, depend on the formation scenario which seems to be very special among the terrestrial planet, as indicated by the Mercury's large bulk density of $\sim$5430 kg/m^{-3}. There are three general hypotheses for the formation of Mercury with its anomalously large density. The first scenario for forming Mercury's large bulk density involves aerodynamic sorting of iron and silicate particles in the solar nebula (Weidenschilling 1978). The other two models for Mercury's formation involve a later stage loss of silicate, and retention of iron, either by stripping of the outer, silicate layers of a larger, differentiated, proto-Mercury by an impact (e.g., Cameron et al. 1988; Wetherill 1988) or by a more exotic scenario that involves a late-state vaporization of silicates (Fegley and Cameron 1987).

Based on different formation scenarios, Taylor and Scott (2005) proposed several composition models that satisfy both the high density of Mercury and the low FeO content of its mantle (see also Van Hoolst et al. in this book). They differ strongly in relative content in olivine, pyroxenes and garnet and in the amount of radiogenic elements; leading to the possibility that measurements performed by the future missions MESSENGER and Bepi-Colombo may strongly constrain the bulk composition of Mercury and potentially its mode of formation.

4.1 Early Thermal State of Mercury

The earliest thermal state of Mercury depends on two main processes: the accretion of the planet by extraterrestrial impacts and core formation and the associated release of gravitational potential energy during metal-silicate differentiation. Both processes may have occurred during the first few ten's of million years of the planet's evolution, as is suggested for Mars and Earth (e.g., Kleine et al. 2002). Accretion of material during the formation of planets is likely one of the largest sources of heat. The accretional heat is the energy accumulated during the burial of heat by impacts as the planet grows through the accretion of planetesimals. During accretion a temperature profile is generated where the temperature increases from the center towards the surface. This accretional energy is sufficient to melt the entire planet. However, the fraction of the available accretional energy that is retained inside the planet instead of radiating away is not known, but only 20% would suffice to ensure accretional melting of nearly all of Mercury (Schubert et al. 1988).

Core formation, the result of separation of metal from silicate materials due to differences in their densities, most likely occurred contemporaneously with or shortly after a planet's accretion. Recent studies on short-lived radio-nuclides (e.g., ^{182}Hf) suggest that the separation between silicates and iron occurred on sampled terrestrial bodies on the order of 1–5 $\times$ 10^7 years after accretion (e.g., Kleine et al. 2002). Planets are assumed to have initially accreted as a mixture of silicate and metal particles, based largely on the composition of chondrites. However, it is likely that at the late stage of accretion the planetesimals were already differentiated (e.g., Kleine et al. 2004; Baker et al. 2005). Estimates of the time scale of the core formation process suggest that for rapid separation both the silicate and the iron need to be fluid at least in the upper part of the planet (e.g., Stevenson 1990). The gravitational energy released by core formation is converted into thermal energy, which strongly heats the interior. During core formation, when iron sinks to the center, the temperature profile is inverted to decrease from the center towards the surface. The total energy released by the differentiation of a homogeneous planet into an iron-rich core and a silicate mantle can be estimated from the difference between the potential energy stored in a homogeneous planet after accretion and the potential energy of the differentiated, two-layer planet. If this energy is homogeneously distributed in the planetary interior—that is, if there is thermal equilibrium between the mantle and the core—estimates for the mean temperature increase are about 700 K for Mercury (Solomon 1979). Formation models that assume a large impact that stripped of the outer, silicate layers of a larger, differentiated, proto-Mercury or a late-state vaporization of silicates would suggest a much stronger temperature increase. In these models, the planetary radius at the time of core formation was larger and thus, the associated potential energy higher. On the other hand, the potential energy released by core formation may be smaller for a heterogeneous accretion in which planetesimals are already differentiated.

It is also likely that due to the assumed rapid core formation process the core was superheated with respect to the mantle. The excess temperature can be the consequence of adiabatic heating of the sinking iron since the core alloy has a thermal expansion coefficient which is 2–3 times larger than that of mantle silicates. Furthermore, the order of magnitude higher thermal conductivity of iron in comparison to silicate allows more efficient heating of the sinking iron blobs by viscous dissipation than of the silicate mantle through which the iron sinks.

In addition to the two main processes that provide early internal heating and differentiation, other energy sources may have contributed to the early heat budget such as the decay of short-lived radioactive isotopes like Al^{26} (Lee et al. 1976), electromagnetic heating (Sonett

Table 1 Adopted models for the abundances of heat-producing elements in the silicate fraction of Mercury from the various formation scenarios

Model	U (ppb)	Th (ppb)	K (ppm)
Condensation[(1)]	30	120	0
Late impact[(2)]	8	30	550
Vaporization[(3)]	0	400	0

[(1)] (Weidenschilling 1978) [(2)] (Cameron et al. 1988; Wetherill 1988) and [(3)] (Fegley and Cameron 1987). For further description of the models see Sect. 4.2

et al. 1975) and tidal dissipation. In conclusion, a hot initial state of Mercury with early core formation is the most likely scenario for Mercury. The exact temperatures are unknown, although it is often assumed that the temperature after core formation is close to the mantle solidus and to the liquidus adiabat in the core (Stevenson et al. 1983; Schubert et al. 1988; Spohn 1991). However, a heterogeneous accretion for Mercury may also imply cooler core temperatures that are below the core liquidus (Hauck et al. 2004).

4.2 Radioactive Heat Source Density

The three general hypotheses for the formation of Mercury also yield predictions for the abundances of the important heat-producing elements uranium (U), thorium (Th), and potassium (K) (Table 1). Therefore, though the elemental composition of the planet is unknown, the predictions of each of these scenarios for Mercury's formation can inform understanding of the amount of heat potentially produced within the planet over time. The aerodynamic sorting of iron and silicate particles in the solar nebula (Weidenschilling 1978) might have given the planet abundances of U and Th similar to the upper mantle of the Earth, though lacking much K (Basaltic Volcanism Study Project 1981). A large impact that strips off the outer, silicate layers of a larger, differentiated, proto-Mercury (e.g., Cameron et al. 1988; Wetherill 1988) could have left a silicate layer with near CI chondritic abundances of heat-producing elements (e.g., Lodders and Fegley 1998). A late-state vaporization of silicates would result in a Th-rich silicate layer lacking appreciable U and K (Fegley and Cameron 1987).

4.3 Mantle Viscosity

The rheology of the mantle is a primary factor affecting convection in terrestrial planets and a prerequisite for convection is that the material behaves like a fluid (i.e., flows under small differential stresses). The timescale over which the mantle is fluid-like is of utmost importance. Over short timescales the mantle is approximately elastic, consistent with the transmission of seismic waves, but over periods longer than $\sim$1000 years the mantle behaves like a fluid with a viscosity that depends on the magnitude of the high temperatures and pressures. Unfortunately, such conditions, particularly the low strain rates, cannot be reproduced in the laboratory and thus the assumed rheology of planetary mantles is primarily based on extrapolation of experimental studies and analysis of terrestrial geodetic data. What is known is that the viscosity of mantle rocks under the wide variety of conditions in planetary mantles is dependent on temperature, pressure, stress, grain size, and composition.

The exponential dependence of the viscosity on the inverse absolute temperature is the most important parameter for understanding the role of mantle convection in transporting

heat. The temperature dependence of the viscosity acts as a thermostat to regulate the mantle temperature. Any tendency of the mean temperature to increase is offset by an associated reduction in mantle viscosity, an increase in convective vigour, and a more efficient outward transport of heat. Similarly, a decrease in mantle temperature tends to increase mantle viscosity, reduce convective flow velocities, and decrease the rate of heat transfer. As a result of the sensitive feedback between mantle temperature and rheology, relatively small changes in temperature can produce large changes in heat flux, and the temperature is consequently buffered at nearly constant temperature (Tozer 1965).

In addition to the temperature dependence, the rheology in a planetary mantle can be described by two main creep mechanisms—diffusion creep and dislocation creep. For the case of diffusion creep the solid behaves as a Newtonian fluid where the viscosity is independent of the applied shear stresses. In contrast, for dislocation creep, the solid behaves as a non-Newtonian fluid where viscosity depends on shear stress. Indeed, viscosity tends to decrease with increasing shear stress, often nonlinearly. Which creep mechanism is valid in Mercury's mantle is not certain. Most laboratory studies of mantle deformation have concluded that dislocation creep is the applicable deformation mechanism in the upper Earth mantle and diffusion creep in the lower mantle (see Schubert et al. 2001). However, this assumption is not consistent with post-glacial rebound studies that favour diffusion creep for the upper mantle, too. Furthermore, laboratory measurements have shown that the pressure-dependence on viscosity cannot be neglected in a terrestrial mantle (Karato and Rubie 1997); even for the thin Mercury mantle. Thus, the viscosity of a terrestrial mantle can be described with the following relationship:

$$\eta = \frac{C}{\tau^{n-1}} \exp\left(\frac{A + pV}{RT_m}\right). \tag{4}$$

Here C is a constant, τ is the stress tensor, n is the stress exponent ($n = 1$ for Newtonian rheology and a typical value of n is 3.5 for a non-Newtonian rheology), T_m is the mean temperature of the convecting fluid, R is the universal gas constant, A is the activation energy for creep (e.g., Weertman and Weertman 1975), p is the pressure and V is the activation volume. The values of the activation energy and volume depend on the mineralogical composition, which is basically unknown for Mercury and as mentioned earlier depends also on the formation scenario. However, should Mercury's mantle contain olivine then it would likely dominate the rheology of the silicate mantle (e.g., Karato and Wu 1993). It has been generally assumed that the Mercurian mantle is volatile-poor because of its refractory nature (Schubert et al. 1988). A dry mantle is also favored from thermal evolution models to explain the small planetary contraction (Hauck et al. 2004). For dry olivine, an activation energy of about 540 kJ/mole at pressures of 12 GPa (Karato and Wu 1993) and an activation volume of about 15 cm^3/mol (Karato and Rubie 1997) can be assumed. To obtain C for Newtonian rheology, a reference viscosity of about 10^{21} Pa s at a temperature of 1,600 K can be used. This value is typical for the upper Earth mantle and often used also for other terrestrial mantles (e.g., Schubert et al. 1988; Nimmo and Stevenson 2000; Breuer and Spohn 2003). It has been speculated, however, that the mantle of Mercury might be even stiffer than the Earth's mantle at the same temperature and pressure because of its refractory and volatile poor composition (Schubert et al. 1988), thus even a higher reference viscosity might be possible.

4.4 Thermal Properties of Mantle and Crust

The thermal conductivity depends on various factors like temperature, pressure, composition, and texture of the material. In the mantle, the phonon contribution, k_{lat}, and the radiative

contribution, k_{rad}, contribute to the thermal conductivity.

$$k_m(T, P) = k_{\mathrm{lat}}(T, P) + k_{\mathrm{rad}}(T). \tag{5}$$

The phonon contribution k_{lat} decreases with increasing temperature and increases with increasing pressure, whereas the radiative contribution k_{rad} increases with increasing temperature independent of pressure; for relevant temperatures in a terrestrial mantle, the phonon conductivity is much higher than the radiative contribution. As a consequence, a decrease of the thermal conductivity through the upper mantle and an increase through the lower mantle is expected. Hofmeister (1999) developed a model describing the temperature and pressure dependence of the mantle thermal conductivity under terrestrial conditions. Using this model for Mercury suggests that the thermal conductivity in the convecting mantle ranges between 2.7 and 3.5 $\mathrm{W\,m^{-1}\,K^{-1}}$, a value below the usually assumed value of 4 $\mathrm{W\,m^{-1}\,K^{-1}}$.

The crust of the terrestrial planets can act as a thermal insulator for the planet. First, it is enriched in radioactive elements and second its thermal conductivity is lower than that of mantle material. The thermal conductivity of the majority of compact volcanic materials ranges between 1.5 and 3.5 $\mathrm{W\,m^{-1}\,K^{-1}}$ at ambient temperatures (Clifford and Fanale 1985; Clauser and Huenges 1995) but decreases with temperature, similar to mantle material (Seipold 1992). For example, the thermal conductivity of typical compact basalt decreases from about 2 $\mathrm{W\,m^{-1}\,K^{-1}}$ at 270 K to about 1.5 $\mathrm{W\,m^{-1}\,K^{-1}}$ at 800 K. In addition to the temperature effects on the thermal conductivity, the structure of the material can change the thermal conductivity significantly. Fractured and porous materials have a reduced thermal conductivity in comparison to compact material. The upper crust of Mercury been fractured due to impact processes, in particular in the early period of heavy bombardment. These impacts resulted in the production of a porous megaregolith that extends to considerable depths. At the transition between fractured and coherent basement, the lithostatic pressure is sufficient to close all fractures and the intergranular pore space. The megaregolith extends to about 10 km for Mars and as the lithostatic pressure for Mars is similar to Mercury also a similar depth of the megaregolith can be assumed. It is expected that the porosity decreases exponentially from the dusty surface to this self-compaction depth (Binder and Lange 1980). As a consequence, the thermal conductivity decreases from the bottom of the megaregolith toward the surface. At low atmospheric pressures like Mercury's, the thermal conductivity at the surface can exhibit extremely low values. Remote thermal measurements for the Martian surface indicate soil thermal conductivities in the range of 0.075 to 0.11 $\mathrm{W\,m^{-1}\,K^{-1}}$ (Kieffer 1976).

4.5 Melting Temperature of the Mantle and the Core

The melting temperature of the mantle and core depends on its chemical composition. Although the mineralogy of Mercury's mantle can be very different from the composition of the terrestrial upper mantle, dominated by peridotite rocks, the solidus of the KLB-1 peridotite (Zhang and Herzberg 1994) is usually assumed in thermo-chemical evolution models of Mercury (Conzelmann 1999; Hauck et al. 2004). Several recent experiments show indeed that the solidus temperature is quite insensitive to both mineralogical and iron contents (Bertka and Holloway 1993; Hirschmann 2000; Herzberg et al. 2000; Schwab and Johnston 2001).

Mercury's core, by analogy with Earth, is thought to be made up of an alloy of Fe–Ni and another light element. Based on cosmochemical models for Mercury's formation (e.g.,

Basaltic Volcanism Study Project 1981; Wetherill 1985; Lewis 1988) sulfur is a likely candidate for that light element and it has received considerable attention in modelling efforts (e.g., Stevenson et al. 1983; Schubert et al. 1988: Harder and Schubert 2001; Hauck et al. 2004). Increasing amounts of sulfur in the core alloy, up to the eutectic point, result in a corresponding depression in the melting point (e.g., Usselman 1975; Boehler 1992; Fei et al. 1997). Sulfur would be essentially insoluble in a solid iron inner core, hence inner core growth leads to an increase in the concentration of sulfur in the outer core, via mass balance, and therefore a moderation of further growth due to increased melting point depression. Indeed, even a minimal amount of sulfur could stave off complete solidification of the core because that would require core mantle boundary temperatures falling below the Fe–FeS eutectic point of ∼1,260 K. Consequently, models of Mercury's internal evolution that account for the presence of sulfur as an alloying element in the core predict that total amounts of inner core growth decrease with increasing total bulk core sulfur content (Stevenson et al. 1983; Schubert et al. 1988; Hauck et al. 2004).

To calculate the growth of an inner core in thermal evolution models, the decrease in the melting temperature due to the increase of sulfur in the outer core needs to be considered. At present, only the melting temperatures of pure iron (e.g., Boehler 1996) and the eutectic composition (e.g., Boehler 1996; Fei et al. 1997, 2000) have been measured. Thus, a parameterization for the melting depression with increasing sulfur at constant pressure is required Note that the melting temperatures for the eutectic composition differ between the work of Boehler (1996) and of Fei et al. (1997, 2000); therefore, different parameterizations exist for the two data sets (see Appendix and Table 3). Furthermore, the parameterizations all use melting curves that have a linear-dependence on sulfur content, which is probably not the case. Thus, the melting points used are probably underestimates of the true melting temperature except for pure Fe and eutectic Fe–FeS.

5 Mantle Dynamics and the Thermo-Chemical Evolution of the Mantle and the Core

5.1 Conduction versus Convection in the Mercury Mantle

The question of whether mantle heat transport in Mercury occurs by conduction or convection is controversial, and depends mainly on the assumption about the initial thermal state, the amount and distribution of radioactive elements, and the efficiency of heat transport. Early models that assume an undifferentiated, and thus cold Mercury, show that the planet cools conductively throughout its evolution (e.g., Siegfried and Solomon 1974; Fricker et al. 1976; Sharpe and Strangway 1976; Solomon 1976, 1977, 1979). Models that assume an initially hot and fully differentiated Mercury are in favour of convection (Solomon 1977; Stevenson et al. 1983; Schubert et al. 1988). This assumption has been confirmed by axial symmetric convection models with a temperature- and pressure-dependent and Newtonian viscosity and a radioactive heat source density consistent to the formation model of silicate vaporization (Conzelmann 1999). The results show that thermal convection is likely during the entire evolution of the planet although it can be very sluggish at present. Recent studies (Solomatov and Reese 2001; Hauck et al. 2004) that have considered a non-Newtonian rheology and crustal formation suggest an initially convecting mantle only during the early stages of evolution accompanied by extensive melting and differentiation. At some later time convection and melting cease and the planet cools in a conductive regime. The more crust produced and the more the mantle is depleted in heat sources the more likely (and earlier) the transition from a convective to a

Table 2 Parameter values used for the 2D axis-symmetric and 3D spherical convection models

Planet radius	r_p	$2{,}440 \times 10^3$ m
Core radius	r_{CMB}	$1{,}900 \times 10^3$ m
Shell thickness	d	540×10^3 m
Gravity	g	3.8 m/s^2
Mantle density	ρ_m	3,060 kg/m^3
Mantle heat capacity	C_m	1,297 J/kg K
Thermal expansivity	α	2.0×10^{-5} 1/K
Thermal conductivity	λ	4 W/K
Viscosity	η_{ref}	8.7×10^{22} Pa s
Activation energy	E_{act}	466.07 kJ/mol
Activation volume	V_{act}	7.43 cm^3/mol
Initial temperature contrast	ΔT	1,660 K
Surface temperature	T_{surf}	440 K
Initial temperature at mid-depth	T_{int}	1,700 K
Initial core temperature	T_{CMB}	2,100 K
Initial internal heating rate	Q_0	5.2373×10^{-8} W/m^3
Radioactive decay rate	σ	0.04951 Ga
Rayleigh number	Ra	698
Core density	ρ_c	8,380 kg/m^3
Core heat capacity	C_c	750 J/kg K
Iron density at core pressure	ρ_{ic}	8,412.27 kg/m^3
Sulfur density at core pressure	ρ_s	6,077.78 kg/m^3

conductive regime. This transition can be retarded or does not take place when the temperature dependence of the mantle conductivity is considered together with the isolating effect of a low-conductivity crust (Breuer 2006). The importance of the temperature dependence of the mantle conductivity and the isolating effect of a low-conductivity crust has already been demonstrated for the thermal evolution of Mars (Schumacher and Breuer 2006).

To study how a present-day convective structure would look, assuming a Newtonian rheology and sufficient heat sources are left in the present mantle of Mercury or a strong thermal isolation of the crust, we have performed 2D axial and 3D spherical convection models with a strongly temperature-dependent and Newtonian viscosity and using the parameters in Table 2 (Figs. 1, 3, 4, 5, 6 and 7). The results show the rapid growth of a thick stagnant lid (Fig. 3). The upper thermal boundary layer comprises nearly half of the mantle, thus mantle convection is restricted to a thin layer of about 250 to 300 km (Fig. 4). The convection pattern in the remaining convecting layer is dominated by small scales of degree 16 to 20 (Fig. 1). However, the convection pattern might be more large scale in the case of strongly pressure-dependent viscosity (Conzelmann 1999). Due to the small temperature gradient at the core–mantle boundary (Fig. 4), cold downwellings (instead of warm plumes) determine the flow pattern. One possibility to learn whether the Mercurian mantle is convecting, in addition to numerical modelling of the mantle flow, is the determination of the mantle structure and the core–mantle boundary shape with gravity and topography data.

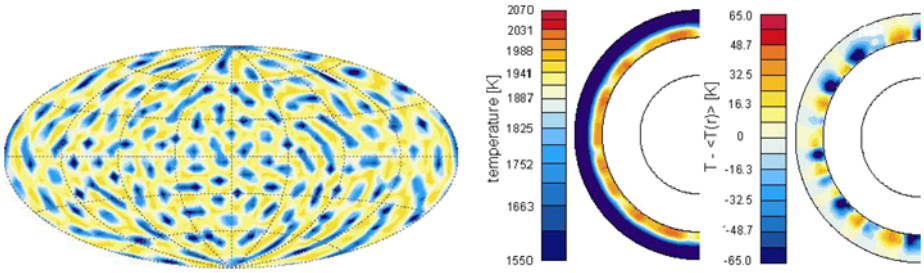

Fig. 1 Present-day convection pattern for an illustrative thermal evolution scenario calculated form an axis-symmetric model with temperature- and pressure-dependent Newtonian viscosity and a growing inner core (detailed description of the model is given in Sect. 3.2 and Appendix) with 1 wt% S in the core (melting curve parameterization based on data by Boehler (1996); see Table 3); silicate heat production given by Th abundances for a vaporization-dominated composition (see Table 1); and an initial mantle temperature of 1,700 K. *Left figure*: the radial velocity at $r = 1{,}996$ km. *Bluish colours* indicate downward motion, *reddish colours* upward motion. The contour step is 0.47 mm/a. *Middle*: meridional cut through the temperature field ($\phi = 40°$) after 4.5 Ga. *Right*: meridional cut ($\phi = 40°$) of the temperature anomaly ($T - \langle T(r)\rangle$)

Table 3 Parameter values to calculate the melting depression of a Fe–FeS core with increasing sulfur content at different pressure (10)

	a_S	T_{m0}	T_{m1}	T_{m2}
Conzelmann (1999)(1)	2	1835 K	1.215×10^{-11} Pa^{-1}	-8.0×10^{-23} Pa^{-2}
Hauck et al. (2004)(2)	2.4	1809 K	1.54×10^{-11} Pa^{-1}	-11.7×10^{-23} Pa^{-2}

(1) Based on data by Boehler (1996) and (2) based on data by Fei et al. (1997, 2000)

5.2 Mantle Cooling and the Temperature of the Mantle

Similar to the question of whether Mercury's heat transport occurs by conduction or convection, mantle cooling and the temperature distribution depend mainly on the amount of radioactive heat sources and their distribution as well as the efficiency of the heat transport. We discuss the temperature evolution of two illustrative models. First, we examine a parameterized convection model with early mantle convection that later transfers its heat only by conduction (Fig. 2) followed by a finite-amplitude convection model with convection throughout the entire history (Fig. 3).

For the former model, the chosen heat source density is consistent with the composition of the condensation model to explain the high density of Mercury (Table 1). The evolution of mantle and CMB temperatures (Fig. 2a) displays a rapid decrease in temperature from the initial state followed by more moderate cooling paralleling the decay in the concentration of heat-producing elements. The large initial drop in mantle temperature is due to the extraction of a substantial amount of partial melt from the mantle. The associated crust formation depletes the mantle in radioactive heat sources. Mantle convection ceases at about 3.3 Ga, after which CMB temperatures indicate a readjustment in the rate of heat loss due to the change in dominant mechanism of heat transport. An inflection at about 0.8 Ga is due to the energy released on first appearance of a solid inner core (Fig. 2c).

Figure 3 shows the evolution of a temperature profile from a 2D axisymmetric convection model assuming a heat source density consistent with the composition of the vaporization model (Table 1). An initial mantle temperature of 1,700 K has been assumed. Very rapidly,

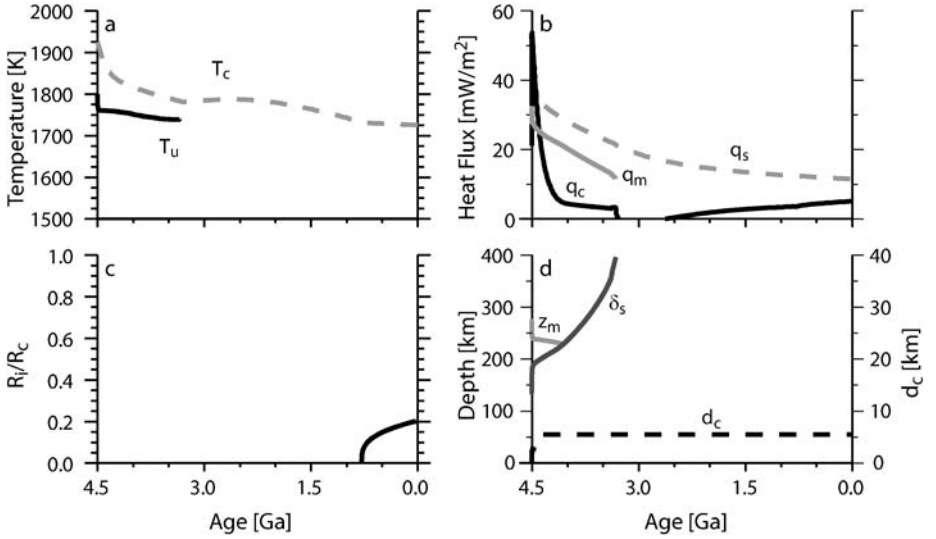

Fig. 2 Illustrative thermal evolution scenario with 8.5 wt% S in the core (melting curve parameterization based on data by Fei et al. (1997, 2000); see Table 2); silicate heat production given by U and Th abundances for a condensation-sequence-dominated composition (see Table 1); a non-Newtonian, pressure-dependent mantle rheology appropriate for dry olivine; partial melting of the mantle and melt transport to the crust; an initial mantle temperature of 1,800 K. (**a**) Temperatures T_c and T_u at the core–mantle boundary and the base of the thermal lithosphere, respectively. (**b**) Heat flux at the surface, q_s, base of the lithopshere, q_m, and core–mantle boundary, q_c. (**c**) Ratio of inner core to outer core radius. (**d**) Greatest depth of pervasive partial melting, z_m, lithospheric thickness δ_s, and crustal thickness, d_c (after Hauck et al. 2004)

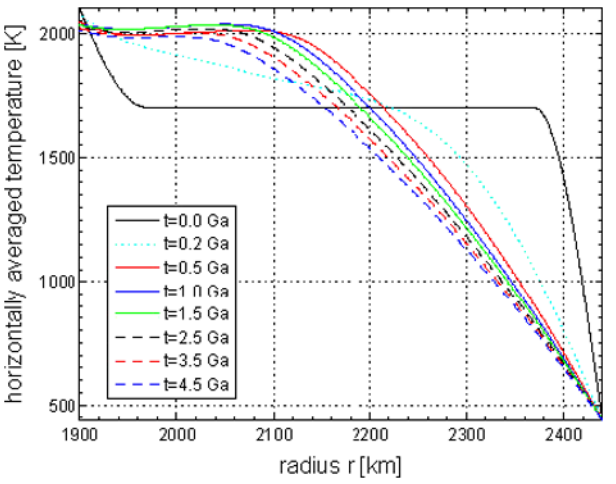

Fig. 3 Temperature profiles at different times in the Mercurian evolution for an axis-symmetric model. For further description see Fig. 1 caption

the lower mantle heats up (temperatures up to 2,026 K are reached) while the upper part cools down. After about 500 Myr, a "final" shape of the temperature profile is reached. In the subsequent evolution, the mantle cools down by thickening the lithosphere which includes the majority of the mantle; convection is restricted to a very thin layer of about 250 km. The temperature of the lower mantle decreases insignificantly and after 4.5 Gyr

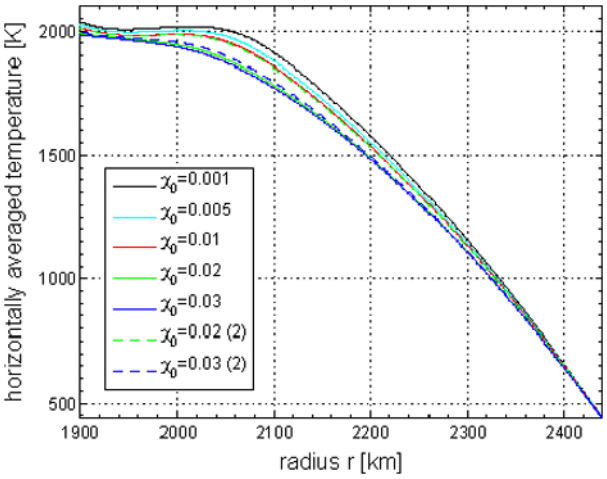

Fig. 4 Temperature profiles after 4.5 Ga for axis symmetric convection simulations with different initial sulfur content and different parameterizations of the melting curve. The initial sulfur content is given in the legend. The *solid lines* refer to the melting curve parameterization based on data by Boehler (1996) and the *dashed lines* refer to the fit of the melting curve using the data by Fei et al. (1997, 2000). For further description see Fig. 1 caption

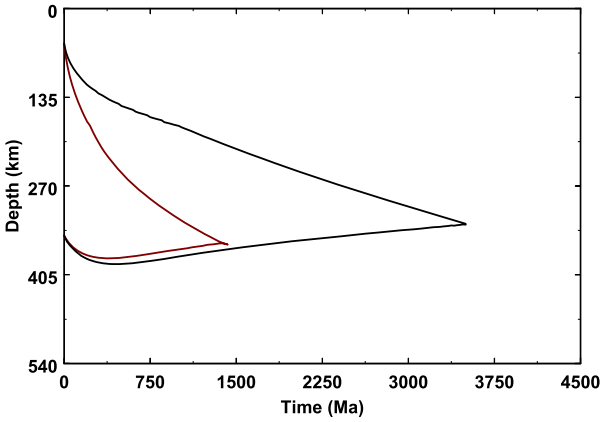

Fig. 5 Extent of partial melt zone in the Mercurian mantle as a function of time for an illustrative thermal evolution scenario with 2 wt% S in the core (melting curve parameterization based on data by Boehler 1996; see Table 2); silicate heat production given by U and Th abundances for a condensation-sequence-dominated composition (see Table 1); a Newtonian, pressure-dependent mantle rheology appropriate for dry olivine; partial melting of the mantle and melt transport to the crust; an initial mantle temperature of 1,800 K. (*Red lines*) constant thermal conductivity in crust and mantle of 4 $W/m^{-1}\,K^{-1}$ and (*black lines*) a low-conductivity crust with $k_c = 2$ $W/m^{-1}K^{-1}$ and a temperature and pressure dependent thermal conductivity in the mantle according to Hofmeister (1999)

the temperature in the isothermal part is still about 1985 K. The temperature gradient at the CMB is very small consistent with the dominance of cool downwellings in the convection pattern (Figs. 3 and 4).

Variations in bulk core sulfur content also play an important role in influencing the temperature evolution (Fig. 4) of the interior. A variation in the sulfur content leads to different sizes of the solid inner core and, therefore, to a different heat output from the core to the mantle (Fig. 7). The larger the inner core the more gravitational and latent heat due to inner core growth is released during the evolution. At a radius of 2,000 km the temperature is about 80 K higher for the model with a low sulfur content (0.1 wt.%), which shows a big

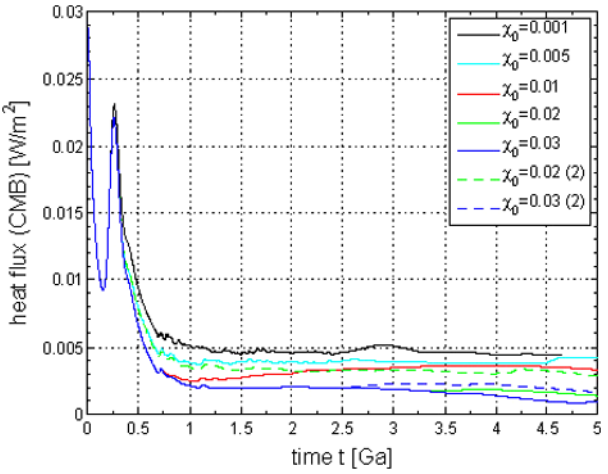

Fig. 6 Heat flux at the core–mantle boundary as a function of time for axis symmetric thermal evolution simulations assuming different initial sulfur contents χ_0. The *solid lines* refer to the melting curve parameterization based on data by Boehler (1996) and the *dashed lines* refer to the fit of the melting curve using the data by Fei et al. (1997, 2000). For further description see Fig. 1 caption

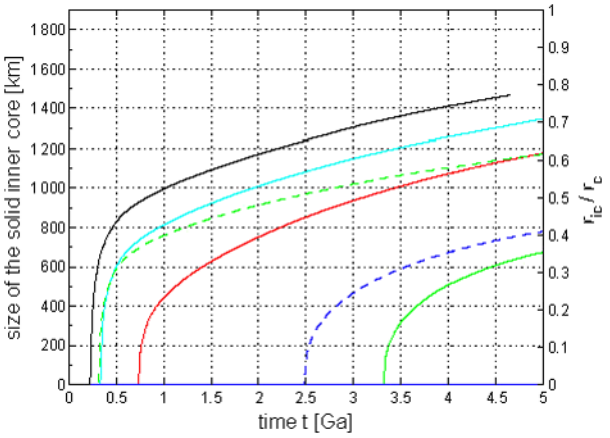

Fig. 7 Evolution of the inner core depending on the initial sulfur content and the parameterization of the melting curve (same legend as in Figs. 4 and 6). For further description see Fig. 1. The *dashed lines* refer to the melting curve parameterization based on the data by Fei et al. (1997, 2000)

inner core (Fig. 7), in comparison to the temperature for the model assuming 3 wt% sulfur in the core. Here, no solid inner core has been formed. The shape of the temperature profiles in the cases with high sulfur content indicates that convection is already quite weak.

5.3 Mantle Partial Melting, Crust Formation and Growth

Formation of crustal material is one of the more important and outwardly visible consequences of terrestrial planet evolution. Primary crustal material, formed from a magma ocean during the latter stages of planet assembly and differentiation, may sequester incompatible heat-producing elements in the crust if no recycling has occurred. On the Earth, most of the present-day crust is the result of extraction of partially melted mantle created during adiabatic decompression of upwelling material. Although Mercury may hold a primary crust, mantle convection there could also result in partial melting if the temperature of upwelling mantle rock exceeds the solidus, leading to formation of secondary crustal material. Effects of crust generated in this manner include a loss of thermal energy in the mantle through the latent heat of fusion and advection of heat as well as enrichment of the

incompatible heat-producing elements in the surface layer, both of which lead to enhanced cooling of the mantle.

One consequence of inefficient heat transfer, particularly on a low-gravity planet like Mercury, is that average, sub-lithospheric temperatures may be pervasively above the solidus (e.g., Reese et al. 1998; Solomatov and Moresi 2000; Hauck and Phillips 2002; Hauck et al. 2004). This infers that any upwelling through such a region would result in generation of partial melt, as confirmed by the 2D and 3D convection models (e.g., Conzelmann 1999 and Fig. 3). The evolution of these models shows that partial melt is present in the deep mantle below the stagnant lid for a significant time. However, if mantle cooling due the extraction of partial melt and the depletion of the mantle in radiogenic heat sources is very strong, it is likely that the generation of partial melt is limited to the early evolution (Solomatov and Reese 2001; Hauck et al. 2004; Fig. 2d). This cooling effect may be compensated by the thermal insulation of a low-conductivity crust and possibly by tidal dissipation in a partially molten mantle. In the case where the cooling of Mercury's interior is significantly reduced—for example, due to the thermal insulation of the crust—the existence of a partial melt zone deep in the interior may be expanded. Also the temperature dependence of the mantle thermal conductivity (k_m) tends to reduce the efficiency of mantle cooling; thus, models show a much longer existence of a partial melt zone in comparison to evolution models with constant k_m (Fig. 5). Whether melt can still rise from the deep interior to the surface is not certain. For instance, a sluggish convection in the deep mantle may not introduce strong enough stresses for fractures to occur which are necessary for the melt to segregate.

The derived crustal thicknesses of the secondary crust varies between 3–70 km depending on the initial temperature distribution, the assumed amount of radioactive elements and the thermal conductivity in mantle and crust (Hauck et al. 2004; Breuer 2006). These thicknesses are significantly thinner than the estimated crustal thickness for Mercury, varying between 100–300 km (Anderson et al. 1996; Nimmo and Watters 2004; Watters et al. 2005). If one neglects the uncertainties in such models, either a peridotite-dominant mantle is inappropriate or much of the crust is primordial. Recent experiments show that the solidus temperature is quite insensitive to both mineral and iron contents (Bertka and Holloway 1993; Hirschmann 2000; Herzberg et al. 2000; Schwab and Johnston 2001). Thus, it is more likely that a large part of the crust is primordial. Though we lack a comprehensive study of the relative importance of primary versus secondary crust formation on the cooling history of Mercury, any remaining primary crust would have acted to facilitate early and long-term cooling of the planet via sequestration of heat-producing elements near the surface of the planet. This may be inconsistent with the limited amount of radial contraction Mercury may have experienced (Strom et al. 1975; Watters et al. 1998).

5.4 Core Cooling, Solidification and Magnetic Field Generation

Cooling of the metallic core of any terrestrial planet is a major component in its internal evolution; for Mercury it is of tantamount importance due to its large mass fraction of the planet and as a favoured source of the planet's magnetic field. A major aspect of core cooling is the precipitation of solid metallic iron to form a solid inner core from the molten, overlying outer core. Growth of the inner core depends primarily on the rate of cooling of the core by the mantle and the melting relationships of the core materials (i.e., how the melting temperature varies as a function of pressure and composition) (e.g., Stevenson et al. 1983; Labrosse 2003).

Mercury's magnetic field suggests (Ness et al. 1976), though not conclusively (cf. Aharonson et al. 2004), that the planet's core is at least partially fluid. A totally fluid

core, however, is difficult to reconcile with the observed magnetic field because cooling by the mantle alone is likely insufficient to drive convective motions capable of generating a magnetic field. The heat flow is below the critical heat flow along the adiabat of about 11 $\mathrm{m\,W\,m^{-1}\,K^{-1}}$ (Schubert et al. 1988) that is necessary to sustain thermal convection in the core (Stevenson et al. 1983; Schubert et al. 1988; Hauck et al. 2004 and Figs. 2b and 6). Thus, compositional buoyancy generated during inner core growth may be necessary to create the field, which may place an upper bound on the amount of sulfur that the core may host. Depending on the assumed heat source density and its distribution as well as the mantle rheology, the temperature dependence of the mantle thermal conductivity, the thickness of the low-conductivity crust, and tidal dissipation in the mantle, the threshold for the bulk sulfur content (for larger values inner core growth does not begin until after 4.5 Gyr) varies strongly. The more efficient the cooling of the planet's interior, the higher the value of the maximal sulfur content. For instance, Hauck et al. (2004) calculated an upper value of ∼9–10 wt%. Their models assume a pressure-dependent, non-Newtonian rheology and consider crust formation with a depletion of the mantle in radioactive elements; thermal insulation of the crust is not considered. A lower threshold of less than 3 wt% is suggested with the 2D and 3D thermal convection models with a strongly temperature-dependent and Newtonian rheology (Fig. 7) and a heat source density consistent to the silicate vaporization model. These models, however, neglect crust formation and the associated redistribution of radioactive elements. A systematic study is needed to better constrain the upper value.

The evolution of the core size for the latter models is given in Fig. 7. The higher the initial sulfur content, the later the start of the inner core growth, and the smaller is the present size of the inner core. The shown results demonstrate the need for a better understanding of the melting depression between pure iron and the eutectic composition. The parameterization by Hauck et al. (2004) based on data by Fei et al. (1997, 299) leads to higher melting temperatures in comparison to the parameterization by Stevenson et al. (1983) and Conzelmann (1999) based on data by Boehler (1996). In the latter case the inner core formation starts 3 Ga later and the final size of the inner core is 500 km smaller assuming the same bulk sulfur content in the core.

Thermal evolution models for Mercury (Stevenson et al. 1983; Schubert et al. 1988; Conzelmann 1999; Hauck et al. 2004) infer a possible evolution of a dynamo-generated magnetic field. In the early evolution, a dynamo might be generated by thermal convection before the initiation of inner core growth and an associated chemical dynamo. Such an early thermal dynamo, however, could only be active when the core was superheated with respect to the mantle. It is unlikely that a core, which is in thermal equilibrium with the mantle, can start thermal convection and thus dynamo action (Breuer and Spohn 2003). Whether the dynamo action ceases for a time until inner core growth provides sufficient energy depends on the onset time of inner core growth. As shown earlier, the higher the sulfur content the later the onset of inner core growth (Fig. 7). A detection of remnant magnetized crust and the determination of its age with future missions could therefore help to constrain the amount of sulfur in the core and thus the formation scenario.

Like tidal heating in a partially molten mantle, a solid Fe inner core might be capable of generating an amount of tidal dissipation comparable to the heat loss along the adiabat in the outer core. The results by Schubert et al. (1988) show that only a large inner core generates significant heating. However, only 4% of the heat currently leaving the core is the result of tidal heating. Thus, the inner core growth rates and the temperatures are not significantly influenced by this small contribution.

A hydromagnetic dynamo—as assumed in many thermal evolution models—poses a problem in terms of the strength of the calculated field. Although there is presently no satisfying parameterization to calculate the magnetic field strength, estimates suggest a much

larger field than observed (Stevenson et al. 1983; Schubert et al. 1988). Recent thin-shell dynamo models, however, have shown that planets with a large solid inner core (relative inner core size larger than about 0.8) can produce magnetic fields with Mercury-like field intensities (Heimpel et al. 2005; Stanley et al. 2005). Alternatively, a deep dynamo model that suggests a rather small inner core (smaller than 1,000 km in radius) was proposed by Christensen (2006). In this model, the dynamo operates only at depth and the associated dynamo field is strongly attenuated by the skin effect through a stable, conducting region of the upper core. An alternative way of generating a weak magnetic field in Mercury is by a thermo-electric dynamo (Stevenson 1987; Giampieri and Balogh 2002). This dynamo makes use of a thermally derived electromotive force set up at a distorted core–mantle boundary. Such a dynamo requires topography variations of the core–mantle boundary of the order of one kilometer due to mantle convection. Whether this kind of dynamo is active in Mercury cannot be concluded from the current magnetic data. It is, however, possible to detect core–mantle undulations by inversion of the global Mercurian gravity and topography field (Spohn et al. 2001 and Sect. 6). New insights into the magnetic field evolution and the dynamo mechanism of Mercury are expected from the future Mercury missions (see also the chapter by Wicht et al. 2007 in this volume).

5.5 Implications for Planetary Contraction

A major consequence of cooling terrestrial planet forming materials is a reduction in volume. Therefore, estimates of 1–2 km planetary contraction based on surface tectonics (e.g., Strom et al. 1975; Watters et al. 1998) represent an opportunity to constrain the internal history of Mercury via understanding the amounts and rates of cooling consistent with these estimates. Since the Mariner 10 era several workers have constrained a variety of thermal models from purely conductive (e.g., Solomon 1976) to mantle convection (e.g., Schubert et al. 1988) and ones that account for time periods when either mechanism may have dominated (Hauck et al. 2004). A cross-cutting conclusion that can be distilled from these studies is that while the mode of mantle cooling plays an important role in generating planetary contraction either it is not the sole governor of contraction or the estimates of contraction are less than has actually occurred on Mercury, or possibly both.

A significant part of planetary contraction—in addition to the contraction due to the mantle cooling—is the result of cooling the core and the solidification of an inner core. Cooling and complete solidification of an initially fluid core would result in a $\sim$17 km decrease in radius (Solomon 1976). Therefore, Mercury's small amount of inferred contraction is consistent only with a small inner core or a large inner core if most of the inner core was formed before the end of heavy bombardment. The onset time of inner core growth and the inner core size depends on the initial sulfur content (Fig. 7). In general, one can state that the more sulfur in the core the smaller the present inner core size. The observation of a small planetary contraction may provide a lower limit of the sulfur content. For smaller sulfur contents, the planetary contraction obtained after the end of the heavy bombardment and caused by the inner core growth is larger than the observed value of 1 to 2 km. However, the lowest amount of sulfur that is in accord with the small contraction depends also on the efficiency of mantle cooling. Due to mantle regulation of core cooling, slow cooling of the mantle also implies slow core cooling and a smaller solid inner core.

Parameters that control mainly the cooling behaviour of the mantle are the amount and the distribution of radioactive elements, the mantle rheology and conductivity, the thickness of the low-conductivity crust and the amount of tidal dissipation. As the natural radioactive decay of long-lived radioisotopes is the primary source of heat generation in the mantle,

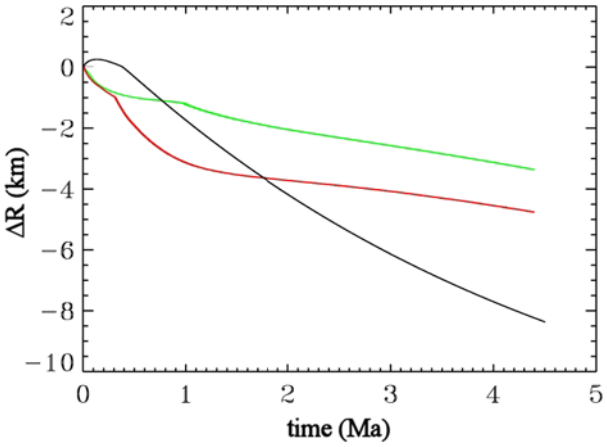

Fig. 8 Contraction of the surface as a function of time for a parameterized convection model based on constant viscosity law (*black line*), for a 2D axisymmetric convection model with strongly temperature dependent viscosity (*red line*) and a 2D axisymmeteric convection model with strongly temperature- and pressure-dependent viscosity (*green line*). The viscosity increases by a factor of 10 in the convecting mantle. Models further assume a concentration of radioactive heat sources consistent to the silicate vaporization model (Fegley and Cameron 1987) and 1% of sulfur in the core (melting curve parameterization based on data by Boehler 1996) (After Conzelmann 1999)

the abundances of these elements (e.g., ^{40}K, ^{232}Th, and ^{235}U, ^{238}U) in the mantle will also tend to mediate total amounts of cooling and cooling rates. An important example is the silicate vaporization scenario for Mercury's high-bulk density that predicts ^{232}Th as the sole source of radiogenic heat (Fegley and Cameron 1987); which, with its 14 Gyr half-life, has not had a significant decline in heat output and hence predicts less cooling and contraction of the planet (Hauck et al. 2004). For models with a significant fraction of the mantle's history being dominated by convection, the effective viscosity of the mantle is a critical parameter controlling the rate of cooling. Higher viscosities tend to result in lower cooling rates, and hence lower amounts of contraction. Under the assumption that olivine is the dominant mantle mineral it is clear that a thoroughly dry mantle is considerably stronger than a wet one (e.g., Karato and Wu 1993). In turn this results in models with a dry olivine mantle viscosity having less, ∼50% or less, contraction than wet olivine models, and the dry models tend to more closely approach the current estimates of total contraction, and therefore recent work has rejected the idea of a wet mantle for Mercury (Hauck et al. 2004).

In fact, it has been suggested that only models assuming a dry Mercurian mantle and the silicate vaporization scenario can explain the small observed contraction with minimal 1–3 wt% sulfur in the core for models without crust formation (Conzelmann 1999; Fig. 8) and at least 6.5 wt-% sulfur if crust formation and a non-Newtonian rheology is considered (Hauck et al. 2004). Enhanced cooling of the mantle due to crust formation can be compensated by the temperature dependence of the mantle thermal conductivity and the inefficient heat transport of a low-conductivity crust (Fig. 5). Depending on the thermal conductivity of the mantle and crustal material, the thickness of the crust, the thickness of the regolith layer, in which the thermal conductivity is significantly reduced in contrast to compact material, mantle cooling can be very inefficient and totally compensate (or even overcompensate) for the enhanced cooling due to crust formation and the depletion of radioactive elements in the mantle. Thus, as long as we do not know the relevant parameter values the sulfur content in the core cannot be restricted.

It is, however, difficult to make concrete conclusions regarding the cooling history of Mercury based merely on current estimates of Mercury's total contraction. Those strain estimates are based upon imagery of only 45% of the surface and do not account for other, potentially subtle, recorders of strain, such as long-wavelength folding. Indeed, Hauck et al. (2004) found that even a factor of two more strain than the current estimates of 0.05–0.10% makes it difficult to discriminate among models even for the concentration of heat-producing elements.

6 Summary and Outlook for Future Missions

We have reviewed our present knowledge of the interior evolution of Mercury. While the known density of the planet gives us at least some knowledge of the gross interior structure (see also chapter by van Holst et al. in this volume), prior to the arrival of MESSENGER and BepiColombo the evolution is largely unconstrained because of a lack of data capable of discriminating between possible evolution scenarios. It is generally agreed from accretion models that Mercury started hot, which also implies early mantle convection (Schubert et al. 1988). The observation of the magnetic field provides probably the best constraint on the interior evolution, assuming that it is generated by a core dynamo and not a remnant field, in that it may indicate a currently convecting outer core.

Another constraint for the interior evolution, although uncertain, is the inferred small planetary contraction from the lobate scarps. The small contraction provides the opportunity to constrain the concentration of radioactive elements, the mantle rheology and the minimal amount of sulfur in the core. Current models suggest that only a dry mantle and Th-rich mantle composition (U and K are strongly depleted) as it is assumed from the silicate vaporization model is consistent with the small planetary contraction of 1 to 2 km. The minimal amount of sulfur, however, remains unconstrained.

The sulfur content in the core depends on the competing effects between efficient cooling of the planet due to crust formation together with the associated depletion of the mantle in radioactive heat sources and inefficient cooling such as the temperature dependence of the mantle thermal conductivity (the thermal conductivity decreases with increasing temperature) and the thermal insulation of a low-conductivity crust. A sulfur content of more than 6.5 wt% is required if one considers cooling by crustal formation (but not its thermal insulation, i.e., the thermal conductivity of the crust is equal to the mantle's conductivity) and a constant mantle thermal conductivity of 4 $\mathrm{W\,m^{-1}\,K^{-1}}$. The threshold of sulfur in that case can be even higher if an enriched primordial crust exists and further enhances the depletion of the mantle in heat sources. These models also suggest a change in the heat transport mechanism. In the early evolution the mantle transport heat by convection but changes later in to a conductive regime. The sulfur content can be as low as 1 wt% in the case of inefficient mantle cooling if the temperature dependence of the mantle thermal conductivity is considered and the crust acts as a thermal insulator. The lower the mantle cooling efficiency the smaller the sulfur content in the core must be in order to explain the observations; furthermore, this low efficiency would also delay any transition to a conductive regime. The efficiency of thermal insulation increases with an increase of the crust thickness and the thickness of the regolith layer. In particular, the regolith layer can exhibit low thermal conductivities that are up to two orders of magnitudes lower than that of the same compact material. In the case of inefficient mantle cooling, mantle convection exists during the entire evolution and a partial melt zone is likely to exist during a substantial period of time in the evolution if not until present.

Mercury's dynamical state is dominated by tidal interaction with the Sun. Thus, it is reasonable to assume that tidal heating might be a heat source in addition to the radioactive heat

sources. Present-day tidal heating in Mercury is a consequence of rotation with respect to the Sun with a period of 87.96 days and the eccentricity of the orbit with a mean eccentricity of 0.206. It is commonly assumed that tidal heating in the mantle is unimportant at the present time (e.g., Schubert et al. 1988). However, this assumption is based on the current understanding that the present mantle is solid and behaves inelastically for tidal forces; the possibility of partial melt has not been adequately considered. Assuming that partial melt in Mercury's mantle was or is still present (Fig. 5), tidal dissipation may contribute to the heat budget of the planet.

Thermal evolution models indicate that the existence of a present-day magnetic field for Mercury is associated with the growth of an inner core—assuming that this field has internal origin. A present-day, purely thermal convection generated dynamo is unlikely since model results show a slow cooling core with less heat flow than can be conducted along the core adiabat (Stevenson et al. 1983; Schubert et al. 1988; Hauck et al. 2004; Figs. 2b and 6). In fact, a thermal dynamo is in general difficult to generate and likely only if the core is superheated with respect to the mantle due to the core formation process. If a thermal dynamo ever existed, it shut off very early in the evolution as the heat flow out of the core decreases rapidly during the first few hundred million years. Whether in the subsequent evolution an inner core can grow and thus a compositional dynamo can be initiated depends strongly on the temperature evolution and the core composition.

At the current stage, only future missions may help to better understand the interior evolution of Mercury. In the following, we present a short overview of the necessary data and what we may learn from them.

6.1 Magnetic Field Data

One of the primary goals of the two missions to Mercury (MESSENGER and BepiColombo) is to clarify the nature of the planet's magnetic field. The data collected by two of Mariner 10's flybys are not conclusive. The BepiColombo mission with its two orbiters, one of them (the Mercury Magnetospheric Orbiter MMO) committed to exploring the magnetosphere and the other (the Mercury Planetary Orbiter) still equipped with a magnetometer is particularly suited to answer that question (Wicht et al., this issue). However, as we discussed earlier, a magnetic field does not necessarily imply a convecting mantle, though a convecting core is likely if the magnetic field originates there, due to the possibility that the inner core growth may power a dynamo while the mantle is conductively cooling. However, convection in the mantle can be indirectly detected by looking for the gravity signal of core mantle boundary undulations and the associated density variations due to mantle convection (see the following).

The magnetometer on board of the MMO will further be able to detect a possible remnant magnetized crust—if one exists at all. Together with a determination of the relative ages of the crust with crater counting, the magnetic field history of Mercury can be obtained. This in turn will help to constrain the sulfur content in the core and the planetary formation scenario.

6.2 Gravity and Topography Data

Radio science and laser altimeters on the orbiters are important instruments for measuring the gravity field and topography. Mercury with its presumably large iron-rich core and thin silicate mantle provides a good candidate to reconstruct the long-wavelength structure of the core–mantle boundary (CMB) from gravity/topography inversion. It is expected that the convective mantle flow induces stresses and thus undulations at the interface (i.e., an inward

deflection below downwellings and an upward below upwellings). Therefore, any information on the CMB shape could provide useful constraints on the mantle dynamics and the proposed thermoelectric dynamo (Stevenson 1987; Giampieri and Balogh 2002). A quantitative study that compared signals generated by the surface topography and CMB topography show that the CMB gravitational signal can be dominant over the surface topography signal at the longest wavelengths ($\ell = 2$–8) (Spohn et al. 2001). For smaller wavelengths as suggested by the convection models described here, the CMB signal is smaller than the crustal gravity signal. Thus, any information about small-scale undulations of the CMB requires a reduction of the crustal field from a measured gravity field. In addition to the difficulty of reducing the crustal field, the model by Spohn et al. (2001) neglects the gravity signal induced by lateral density variations in the convecting mantle, that is, the density is smaller in hot upwellings and larger in cold downwellings as compared to the average value.

Assuming that one is able to remove the crustal field, an inversion method of the reduced measured gravity field, which is caused by density variations in the mantle and by core–mantle undulations, is needed to distinguish between these two contributions. The amplitudes of deformation at the core mantle boundary depend on the strength of convection, which on the other hand depends on mantle viscosity and thermal buoyancy. The latter is caused by density variations due to lateral temperature variations. For Earth, the complete system of a mantle flow and dynamic topography at the boundaries (surface, phase transitions, CMB) has been extensively studied using the framework of internal loading theory (e.g. Hager and Clayton 1989). This method uses surface gravity and topography measurements, density distribution derived from seismic tomography data, and plate velocities to reconstruct the viscosity structure of the mantle. In the case of Mercury, like for other terrestrial planets, the lack of these data does not allow for such an inversion and the ambiguity of the mantle density structure derived from the gravity/topography inversion has to be reduced. One simple approach is to assume a radially averaged (instead of full 3D) structure of the mantle (Pauer et al. 2006).

If such a simplification is employed (Pauer et al. 2007), then properties of such an inversion could be checked through forward/inverse modeling of Mercury's mantle density structure (together with the induced CMB shape) derived from 3D spherical convection models. Such a study shows first of all the dependency of the gravity anomalies amplitudes on the dominant mantle convection pattern wavelength (since the high-degree signal is strongly attenuated as shown in Fig. 9) and on the thickness of an active mantle convection zone (since that is the gravity signal inducing zone). If we are not able to distinguish in the measurements the dynamic surface topography, another unconstrained parameter is then the mantle viscosity profile, which must be chosen a priori. That preliminary study (Pauer et al. 2007) demonstrates that there are two main free parameters, the viscosity profile and the thickness (or depth) of the convecting mantle. These parameters can be constrained together with models of the interior structure and dynamics. In any case future measurements of the gravity field up to degree 20 or even higher will allow us to constrain better the CMB structure.

The forthcoming Mercury missions will provide the J2 gravity term, the obliquity of the rotation axis and the amplitude of libration, data necessary to determine the core radius as outlined by Peale (1988). Though this determination will be non-unique it will provide an additional constraint on the interior structure, the ratio Cm/C. Furthermore, significant progress has recently been made on this front by Margot et al. (2007) who measured the obliquity and amplitude of physical libration using ground-based radar and determined that Mercury's outer core is indeed molten. Future measurements of the degree-two gravitational harmonics by MESSENGER and BepiColombo will significantly improve these results.

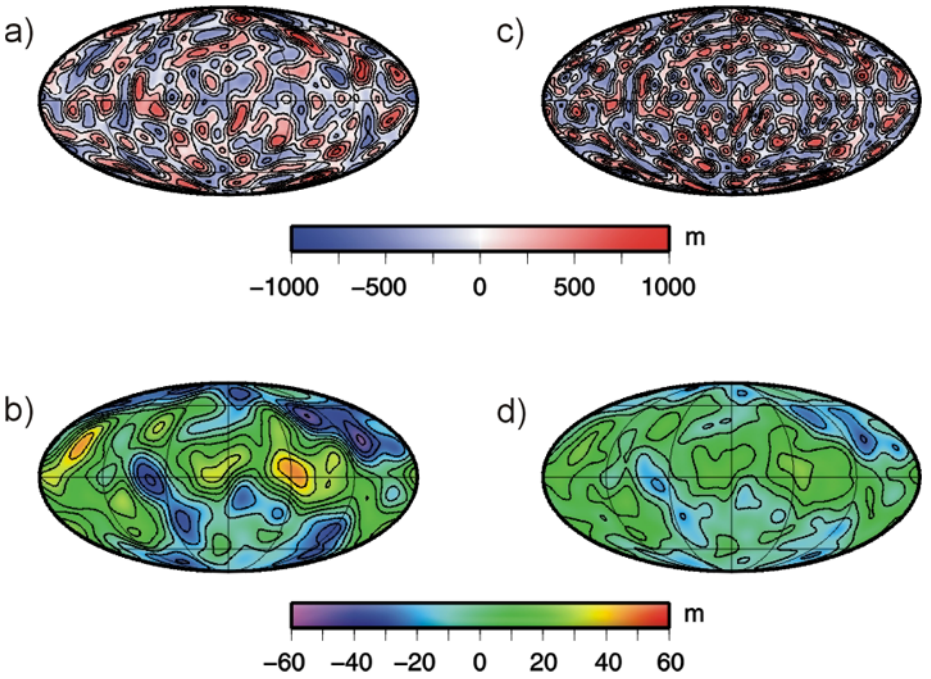

Fig. 9 (**a**) CMB undulations generated by synthetic mantle density distribution dominated by $\ell = 8$ structures (max. anomalies ± 1, 2%) in the model with 300 km thick lithosphere, mantle density 3,350 kg m^{-3}, core radius 1,890 km, core density 8,000 kg m^{-3} and constant mantle viscosity. (**b**) Corresponding surface geoid anomalies. (**c**) Same as for (**a**) but with density distribution dominated by $\ell = 13$ and (**d**) corresponding surface geoid anomalies

BepiColombo will attempt to measure the solar tides of Mercury. With an amplitude of about 1 m the tidal deformation is indeed within the reach of a laser altimeter. This is also true for the gravity signal of the tides. These data will allow a calculation of the tidal Love numbers k and h. The Love numbers are useful as constraints on the interior structure. Their imaginary parts will constrain the rheology of the mantle and possible tidal heating in the mantle. However, it is still doubtful that the time variation of the tidal signal can be accurately resolved. The tides of Mercury also offer the possibility to estimate the sulfur concentration of the core with the precision of a few percent (Van Hoolst et al. 2007, this issue).

The measured gravity field and the topography can also be used to estimate the crustal thickness and the elastic lithosphere (Belleguic et al. 2005). The elastic lithopshere is the upper layer of a terrestrial planet that supports stresses over geologically long periods ($\sim 10^8$ years). Since the base of the elastic (mechanical) lithosphere can be defined by an isotherm which depends on the rheology (composition) and the strain rate (McNutt 1984), its thickness allows estimates of the surface heat flow. It is important to note that the elastic lithosphere obtained by gravity and topography data, does not represent the current state of the thermal lithosphere. It rather shows the thermal state at the time of formation of the considered geological structure. Thus, the elastic lithosphere thickness provides constraints on models of thermal evolution.

6.3 Camera and Spectrometer Data

Cameras together with laser altimeters on both missions will measure tectonic deformations of the crust such as the lobate scarps with an accuracy of a few meters or better on a global scale. As we showed earlier, these measurements are necessary to better constrain the contractional tectonic, and hence the cooling history of the planet. Spectrometers on the Mercury missions will measure the composition and the mineralogy of the crustal rock. These data will be decisive in elucidating the formation scenario and the very early history of the planet. They will also constrain crust growth models through the dependence of the latter on crust physical parameters.

It should be stressed that 55% of the planet is unexplored and that the known 45% have been imaged only at a poor resolution, comparable with lunar images before Apollo. It is entirely possible that hidden in the surface is evidence of the volcanic history of Mercury that will be very important in the light of the theoretical evidence for partial melting in the mantle.

6.4 In Situ Measurements

While MESSENGER and BepiColombo will provide important constraints for models of Mercury's interior it must also be said that many important questions will not likely be solved; these questions will require landers or even networks of landers. The BepiColombo mission for some time planned to include a small lander which was later dropped for technical and financial reasons. Mission studies performed by the European Space Agency have shown that landing on Mercury is extremely difficult and expensive. Nevertheless, the detailed interior structure including the possible asthenosphere can best be studied with the help of seismometers. And the interior energy balance can best be assessed with planetary heat flow measurements.

Appendix

In the 2D axial and 3D spherical convection models presented here the viscosity is strongly temperature dependent, and the viscosity η varies with depth as a function of the horizontally averaged temperature and the lithostatic pressure following an Arrhenius law:

$$\eta = \eta_0 \exp\left(\frac{E_{\text{act}} + V_{\text{act}} g \rho_m (r_p - r)}{R\langle T(r)\rangle}\right), \tag{6}$$

where R is the gas constant, E_{act} the activation energy and V_{act} the activation volume which describes the pressure dependence of the viscosity. η_0 normalizes the profile so that a reference value η_{ref} is reached at mid-depth at a reference temperature of 1,573 K. This viscosity law provides the ability to model the evolution of a stagnant lid, the region of the mantle which does not flow. In that upper layer, heat is transported only by conduction.

A free-slip mechanical boundary condition is used at the CMB and a no-slip condition is implemented at the surface that assures the stagnant lid regime of a one-plate planet. For the temperature boundary conditions, we use a fixed temperature at the surface while the temperature at the CMB decreases according to how much heat is transported out of the core by the mantle. To model the core–mantle temperature, we also solve the energy equation for the core. The cooling of the core is equal to the heat flux out of core (transported by the

mantle) and the energy released if an inner core is growing (mass m), that is, latent heat L and the gravitational energy E_G.

$$V_c \rho_c C_c \frac{\mathrm{d}T_{CMB}}{\mathrm{d}t} = A_c k. \frac{\mathrm{d}T}{\mathrm{d}r}\bigg|_{CMB} - (L + E_G)\frac{\mathrm{d}m}{\mathrm{d}t}, \tag{7}$$

where V_c, A_c, ρ_c and C_c are the volume, the surface, the density and the heat capacity of the core and T_{CMB} is the temperature at the CMB.

The latent heat release per mass is $L = 250\ \mathrm{kJ\,kg^{-1}}$ (Schubert et al. 1988). Gravitational energy contributes to the energy balance because the core contains some light elements like sulfur (see Sect. 2.3). On the iron-rich side of the eutectic composition a pure iron core freezes out and the light component gets enriched and buoyant in the liquid part. We employ the following equation for the gravitational energy given by (Schubert et al. 1988):

$$E_G = \frac{2\pi G r_{CMB}^2 \chi_0 \Delta\rho}{(1-\xi^3)^2}\left(\frac{\rho_{ic}}{\rho_S}\right)\left[\frac{1}{5}\left(1-\xi^5\right) - \frac{\xi^2}{3}\left(1-\xi^3\right)\right], \tag{8}$$

where G is the gravitational constant, $\Delta\rho$ the difference in density between the light component (ρ_S) and the iron (ρ_{ic}). $\xi = r_{ic}/r_{CMB}$ denotes the aspect ratio between the inner core radius (r_{ic}) and the core radius (r_{CMB}) and χ_0 is the initial value of the light element mass concentration in the outer core.

The temperature in the core is assumed to follow an adiabat, so that the radius of the inner core is then determined as the intersection point of the core adiabat and the melting curve for the iron–sulfur alloy. The adiabatic temperature in the core is parameterized as a function of the pressure p (Stevenson et al. 1983):

$$T_{ad}(p) = T_{CMB}\frac{1 + 8\cdot 10^{-12} p - 3.9\cdot 10^{-23} p^2}{1 + 8\cdot 10^{-12} p_{CMB} - 3.9\cdot 10^{-23} p_{CMB}^2}, \tag{9}$$

where p_{CMB} is the pressure at the CMB.

Only the melting temperature of pure iron (Boehler 1996) and the eutectic composition (Boehler 1996; Fei et al. 1997, 2000) has been measured, thus, a parameterization for the melting depression with increasing sulfur at constant pressure is needed. The melting depression of iron due to the light element concentration χ is described in a parameterized melting curve as follows:

$$T_m(p) = T_{m0}(1 - a_S \chi)\left(1 + T_{m1} p + T_{m2} p^2\right), \tag{10}$$

where a_S, T_{m0}, T_{m1}, T_{m2} are constant fitting parameters. With a growing inner core the sulfur content in the liquid shell gets enriched by $\chi = \chi_0 r_{CMB}^3/(r_{CMB}^3 - r_{ic}^3)$. Note that the melting temperatures for the eutectic composition differ between the work of Boehler (1996) and of Fei et al. (1997, 2000) and therefore different parameter values of a_S, T_{m0}, T_{m1}, T_{m2} have to be chosen (Table 3).

To convert the pressure at the intersection point of melting curve and core adiabat into the radius of the inner core a pressure model is needed. Using that the gravity in the core follows $r g_{CMB}/r_{CMB}$ the inner core radius can be derived by the following equation:

$$r_{ic} = \sqrt{2[p(r=0) - p(r=r_{ic})] r_{CMB}/\rho_c g_{CMB}}. \tag{11}$$

In this approach which is used in the here presented models the pressure at the CMB is 6.7 GPa and 42.1 GPa in the center of the planet. The gravity at the CMB g_{CMB} is 4.45 m/s^2.

The different pressure models change the adiabatic temperature structure in the core (using the described parameterization) which gives another source for uncertainty of the size of the inner core. With the lower pressure at the CMB the adiabat gives higher temperatures in the interior, so that the onset of inner core growth is delayed and smaller cores are expected.

The change of the mass of the inner core can be derived from the change of the inner core radius with time:

$$\frac{\mathrm{d}m}{\mathrm{d}t} = 4\pi r_{ic}^2 \rho_c \frac{\mathrm{d}r_{ic}}{\mathrm{d}t} = 4\pi r_{ic}^2 \rho_c \frac{\mathrm{d}r_{ic}}{\mathrm{d}T_{CMB}} \frac{\mathrm{d}T_{CMB}}{\mathrm{d}t}. \tag{12}$$

The derivative of the inner core radius with respect to the temperature at the CMB can be calculated by equating the melting curve and the adiabat at the transition pressure to the inner core. This expression enters in the energy balance of the core which can be rearranged to a differential equation for the evolution of the temperature of the core in the thermal evolution models.

The initial temperature distribution follows a boundary layer profile with high temperatures in the interior and thin boundary layers. Random small scale disturbances are used to initialize the convection process.

References

M.H. Acuña, J.E.P. Connerney, N.F. Ness, R.P. Lin, D. Mitchell, C.W. Carlson, J. McFadden, K.A. Anderson, H. Rème, C. Mazelle, D. Vignes, P. Wasilewski, P. Cloutier, Science **284**, 790–793 (1999)

O. Aharonson, M.T. Zuber, S.C. Solomon, Earth Planet. Sci. Lett. **218**, 261–268 (2004)

J.D. Anderson, R.F. Jurgens, E.L. Lau, M.A. Slade, III, G. Schubert, Icarus **124**, 690–697 (1996)

J.D. Anderson, G. Colombo, P.B. Esposito, E.L. Lau, G.B. Trager, Icarus **71**, 337–349 (1987)

J. Baker, M. Bizzarro, N. Wittig, J. Connelly, H. Haack, Nature **436**, 1127 (2005)

Basaltic Volcanism Study Project, *Basaltic Volcanism on the Terrestrial Planets* (Pergamon, New York, 1981), 1286 pp

V. Belleguic, P. Lognonné, M.A. Wieczorek, J. Geophys. Res. **110**, E11005 (2005), doi:10.1029/2005JE002437

C.M. Bertka, J.R. Holloway, J. Geophys. Res. **98**, 19,755–19,766 (1993)

A.B. Binder, M.A. Lange, J. Geophys. Res. **85**, 3194–3208 (1980)

R. Boehler, Earth Planet. Sci. Lett. **111**, 217–227 (1992)

R. Boehler, Phys. Earth Planet. Int. **96**, 181–186 (1996)

S.I. Braginsky, Geomag. Aeron. **4**, 698–712 (1964)

D. Breuer, Thermo-chemical evolution of Mercury, EPSC 2006, Berlin, Germany, Sept. 18th–22th, Talk EPSC2006-A-00755, 2006

D. Breuer, T. Spohn, J. Geophys. Res.-Planets **108**(E7), 5072 (2003). doi:10.1029/20002JE001999

D. Breuer, T. Spohn, Planet. Space Sci. **54**, 153–169 (2006)

A.G.W. Cameron, Jr. B. Fegley, W. Benz, W.L. Slattery, in *Mercury*, ed. by F. Vilas et al. (University of Arizona Press, Tucson, 1988), pp. 692–708

C. Christensen, Nature **444**, 1056–1058 (2006)

C. Clauser, E. Huenges, *Thermal Conductivity of Rocks and Minerals, Rock Physics and Phase Relations*, A Handbook of Physical Constants. AGU Reference Shelf 3, 1995

S.M. Clifford, F.P. Fanale, Lunar Planet. Sci. **XVI** 144–145 (1985)

J.E.P. Connerney, N.F. Ness, in *Mercury* (Univ. of Arizona Press, Tucson, 1988), pp. 494–513

V. Conzelmann, Thermische Evolution des Planeten Merkur berechnet unter Anwendung verschiedener Viskositätsgesetze, Ph.D. Thesis, University Münster, 1999

A.C. Cook, M.S. Robinson, J. Geophys. Res. **105** 9429–9443 (2000)

B.M. Cordell, Tectonism and the interior of Mercury, Ph.D. thesis, University of Arizona, Tucson, 1977, 124 pp

B.M. Cordell, R.G. Strom, Phys. Earth Planet. Inter. **15** 146–155 (1977)

A. Davaille, C. Jaupart, J. Fluid Mech. **253** 141–166 (1993)

B. Fegley Jr., A.G.W. Cameron, Earth Planet. Sci. Lett. **82** 207–222 (1987)

Y. Fei, C.M. Bertka, L.W. Finger, Science **275** 1621–1623 (1997)

Y. Fei, J. Li, C.M. Bertka, C.T. Prewitt, Am. Mineral. **85** 1830–1833 (2000)
P.E. Fricker, R.T. Reynolds, A.L. Summers, P.M. Cassen, Nature **259** 293–294 (1976)
G. Giampieri, A. Balogh, Planet. Space Sci. **50** 757–762 (2002)
R. Grard, A. Balogh, Planet. Space Sci. **49** 1395–1407 (2001)
O. Grasset, E.M. Parmentier, J. Geophys. Res. **103** 18,171–18,181 (1998)
L. Grossman, Geochim. Cosmochim. Acta **36**, 597–619 (1972)
B.H. Hager, R.W. Clayton, in *Mantle Convection: Plate Tectonics and Global Dynamics*, ed. by W.R. Peltier (Gordon and Breach, New York, 1989), pp. 675–763
H. Harder, G. Schubert, Icarus **151**, 118–122 (2001)
J.K. Harmon, Adv. Space Res., **19**, 1487–1496 (1997)
S.A. Hauck II, A.J. Dombard, R.J. Phillips, S.C. Solomon, Earth Planet. Sci. Lett. **222**, 713–728 (2004)
S.A. Hauck III, R.J. Phillips, J. Geophys. Res. **107**, 5052 (2002). doi:5010.1029/2001JE001801
M.H. Heimpel, J.M. Aurnou, F.M. Al-Shamali, N. Gomez Perez, Earth Planet. Sci. Lett. **236**, 542–557 (2005)
C.T. Herzberg, P. Raterron, J. Zhang, Geophys. Geochem. Geosyst. **1** (2000). doi:10.129/2000GC000089
M.M. Hirschmann, Geophys. Geochem. Geosyst. **1** (2000). doi:10.129/2000GC000070
A.M. Hofmeister, Science **283**(5408), 1699 (1999)
R. Jeanloz, D.L. Mitchell, A.L. Sprague, I. de Pater, Science **268**, 1455–1457 (1995)
S. Karato, D.C. Rubie, J. Geophys. Res. **102**, 20111–20122 (1997)
S.-I. Karato, P. Wu, Science **260**, 771–778 (1993)
H.H. Kieffer, Science **194**, 1344–1346 (1976)
T. Kleine, C. Münker, K. Mezger, H. Palme, Nature **418**, 952–955 (2002)
T. Kleine, K. Mezger, H. Palme, E. Scherer, C. Munker, AGU, Fall Meeting 2004, Abstract P31C-04, 2004
S. Labrosse, Phys. Earth Planet. Interiors **140**, 127–143 (2003)
T. Lee, D.A. Papanastassiou, G.J. Wasserburg, Geophys. Res. Lett. **3**, 109–112 (1976)
J.S. Lewis, Science **186**, 440–443 (1972)
J.S. Lewis, in *Mercury*, ed. by F. Vilas et al. (University of Arizona Press, Tucson, 1988), pp. 651–666
K. Lodders, B. Fegley Jr., *The Planetary Scientist's Companion* (Oxford University Press, New York, 1998), 371 pp
J.L. Margot, S.J. Peale, R.F. Jurgens, M.A. Slade, I.V. Holin, Science **316**, 710–714 (2007)
C.A. McCammon, A.E. Ringwood, I. Jackson, Geophys. J. Roy. Astron. Soc. **72**, 577–595 (1983)
M.K. McNutt, J. Geophys. Res. **89**, 11180–11194 (1984)
L.-N. Moresi, V.S. Solomatov, Phys. Fluids **7**, 2154–2162 (1995)
N.F. Ness, K.W. Behannon, R.P. Lepping, Y.C. Whang, K.H. Schatten, Science **185**, 151–160 (1974)
N.F. Ness, K.W. Behannon, R.P. Lepping, Y.C. Whang, Icarus **28**, 479–488 (1976)
F. Nimmo, D. Stevenson, J. Geophys. Res. **105**, 11969–11979 (2000)
F. Nimmo, T.R. Watters, Geophys. Res. Lett. **31**, L02701 (2004)
M. Pauer, O. Fleming, K. Čadek, J. Geophys. Res. **111**(E11), E1100 (2006). doi:10.1029/2005JE002511
M. Pauer, D. Breuer, T. Spohn, Subsurface structure of Mercury—Expected results from gravity/topography analyses (2007, submitted)
S.J. Peale, in *Mercury*, ed. by F. Vilas et al. (University of Arizona Press, Tucson, 1988), pp. 494–513
C.C. Reese, V.S. Solomatov, L.N. Moresi, J. Geophys. Res. **103**, 13643–13658 (1998)
C.C. Reese, V.S. Solomatov, L.-N. Moresi, Icarus **139**, 67–80 (1999)
F.M. Richter, H.C. Nataf, S.F. Daly, J. Fluid Mech. **129**, 183 (1983)
A.E. Ringwood, Geochem. J. **11**, 111–135 (1977)
M.S. Robinson, M.E. Davies, T.R. Colvin, K.E. Edwards, J. Geophys. Res. **104**, 30 (1999)
M.S. Robinson, G.J. Taylor, Meteorit. Planet. Sci. **36**, 841–847 (2001)
S.K. Runcorn, Nature **253**, 701–703 (1975)
C.T. Russel, D.N. Baker, J.A. Slavin, in *Mercury*, ed. by F. Vilas, C.R. Chapman, M.S. Matthews (Univ. Press of Arizona, Tucson, 1988), pp. 514–561
G. Schubert, M.N. Ross, D.J. Stevenson, T. Spohn, in *Mercury*, ed. by F. Vilas et al. (Univ. Press of Arizona, Tucson, 1988), pp. 429–460
G. Schubert, D. Bercovici, G.A. Glatzmeier, J. Geophys. Res. **95**, 14105–14129 (1990)
G. Schubert, S.C. Solomon, D.L. Turcotte, M.J. Drake, N.H. Sleep, in *Mars*, ed. by H.H. Kieffer, B.M. Jakobsky, C.W. Snyder, M.S. Matthews (University of Arizona Press, Tucson, 1992), pp. 147–183
G. Schubert, D.L. Turcotte, P. Olson, *Mantle Convection in the Earth and Planets* (Cambridge University Press, Cambridge, 2001), 956 pp
S. Schumacher, D. Breuer, J. Geophys. Res. **111**, E02006 (2006). doi:10.1029/2005JE002429
B.E. Schwab, A.D. Johnston, J. Petrol. **42**, 1789–1811 (2001)
U. Seipold, Phys. Earth Planet. Int. **69**(3–4), 299-303 (1992)
H.N. Sharpe, D.W. Strangway, Geophys. Res. Lett. **3**, 285–288 (1976)
R.W. Siegfried, S.C. Solomon, Icarus **23**, 192–205 (1974)

D.E. Smith, M.T. Zuber, G.A. Neumann, F.G. Lemoine, J. Geophys. Res. **102**, 1591–1611 (1997)
V.S. Solomatov, Phys. Fluids **7**, 266–274 (1995)
V.S. Solomatov, L.-N. Moresi, J. Geophys. Res. **105**, 21795–21817 (2000)
V.S. Solomatov, C.C. Reese, Mantle convection and thermal evolution of Mercury reviseted, in *LPI Conference Mercury: Space Environment, Surface, and Interior*, Chicago, 2001
S.C. Solomon, Icarus **28**, 509–521 (1976)
S.C. Solomon, Phys. Earth Planet. Inter. **15**, 135–145 (1977)
S.C. Solomon, Earth Planet. Sci. Lett. **19**, 168–182 (1979)
S.C. Solomon, R.L. McNutt Jr., R.E. Gold, M.H. Acuña, D.N. Baker, W.V. Boynton, C.R. Chapman, A.F. Cheng, G. Gloeckler, J.W. Head III, S.M. Krimigis, W.E. McClintock, S.L. Murchie, S.J. Peale, R.J. Phillips, M.S. Robinson, J.A. Slavin, D.E. Smith, R.G. Strom, J.I. Trombka, M.T. Zuber, Planet. Space Sci. **49**, 1445–1465 (2001)
C.P. Sonett, D.S. Colburn, K. Schwartz, Icarus **24**, 231–255 (1975)
T. Spohn, F. Sohl, K. Wieczerkowski, V. Conzelmann, Planet. Space Sci. **49**, 1561–1570 (2001)
T. Spohn, Icarus **90**, 222–236 (1991)
A.L. Sprague, R.W.H. Kozlowski, F.C. Witteborn, D.P. Cruikshank, D.H. Wooden, Icarus **109**, 156–167 (1994)
A.L. Sprague, D.B. Nash, F.C. Witteborn, D.P. Cruikshank, Adv. Space Res. **19**, 1507–1510 (1997)
P.D. Spudis, J.E. Guest, in *Mercury*, ed. by F. Vilas et al. (University of Arizona Press, Tucson, 1988), pp. 118–164
S. Stanley, J. Bloxham, W.E. Hutchinson, M.T. Zuber, Earth Planet. Sci. Lett. **234**, 27–38 (2005)
D.J. Stevenson, Earth Planet. Sci. Lett. **82**, 114–120 (1987)
D.J. Stevenson, in *Origin of the Earth*, ed. by H.E. Newsom, J.H. Jones (Oxford University Press, New York, 1990), pp. 231–249
D.J. Stevenson, T. Spohn, G. Schubert, Icarus **54**, 466–489 (1983)
R.G. Strom, Adv. Space Res. **19**, 1471–1485 (1997)
R.G. Strom, N.J. Trask, J.E. Guest, J. Geophys. Res. **80**, 2478–2507 (1975)
G.J. Taylor, E.R.D. Scott, in *Treatise on Geochemistry, vol. 1, Meteorites, Comets and Planets*, ed. by M.A. Davis (Elsevier, Amsterdam, 2005), pp. 477–485
M.N. Toksöz, A.T. Hsui, D.H. Johnston, Thermal evolution of the Moon and the terrestrial planets, in *The Soviet–American Conference on Cosmochemistry of the Moon and Planets*, NASA SP-370, 1978, pp. 245–328
D.C. Tozer, Phil. Trans. Roy. Soc. **258**, 252–271 (1965)
T.M. Usselman, Am. J. Sci. **275**, 278–290 (1975)
T. Van Hoolst, F. Sohl, I. Holin, O. Verhoeven, V. Dehant, T. Spohn (2007), this issue
F. Vilas, in *Mercury*, ed. by F. Vilas, C.R. Chapman, M.S. Matthews (University of Arizona Press, Tucson, 1988), pp. 622–650
T.R. Watters, M.S. Robinson, A.C. Cook, Geology **26**, 991–994 (1998)
T.R. Watters, R.A. Schultz, M.S. Robinson, A.C. Cook, Geophys. Res. Lett. **29**(11), 1542 (2002). doi:10.1029/2001GL014308
T.R. Watters, M.S. Robinson, C.R. Bina, P.D. Spudis, Geophys. Res. Lett. **31**, 04701 (2004)
T.R. Watters, F. Nimmo, M.S. Robinson, Geology **33**(8), 669–672 (2005). doi:10.1130/G21678.1
J. Weertman, J.R. Weertman, Annu. Rev. Earth Planet. Sci. **3**, 293–315 (1975)
S.J. Weidenschilling, Icarus **35**, 99–111 (1978)
G.W. Wetherill, Science **228**, 877–879 (1985)
G.W. Wetherill, in *Mercury*, ed. by F. Vilas et al. (University of Arizona Press, Tucson, 1988), pp. 670–691
J. Wicht, M. Mandea, F. Takahashi, U.R. Christensen, M. Matsushima, B. Langlais (2007), this issue
A. Zebib, G. Schubert, J.L. Dein, R.C. Paliwal, Geophys. Astrophys. Fluid Dyn. **23**, 1–42 (1983)
J. Zhang, C. Herzberg, J. Geophys. Res. **99**, 17,729–17,742 (1994)